

**Solar wind – Variability, evolution to Earth
and influence
on the terrestrial magnetic field**

Doctoral thesis in physics

Malte S. Venzmer

University of Göttingen

Institute for Astrophysics

January 2012 – May? 2017

Supervisor:
Dr. Volker Bothmer

Referees:
Prof. Dr. Ansgar Reiners
Prof. Dr. ??

“Despite the ‘Dr.’ before his name, he had completed no course of study and received no degree. When people tried to pin him down about this, he would say that the letters were merely an abbreviation of his first name - Drummond - which he did not use. But it was as ‘Dr.’ Sam Laserowitz that he appeared in a number of science-fiction magazines; he was also known, in the circles of the fans of that genre, as a lecturer, and spoke on ‘cosmic’ themes at their many conferences and convention. Laserowitz’s speciality was earthshaking discoveries, which he happened upon two or three times a year. [...] We really have no idea what a multitude of con men and crackpots inhabit the domain that lies halfway between contemporary science and the insane asylum.”

Excerpt from Stanisław Lem 1968, *His Master’s Voice* ([Lem & Kandel 1984](#), p. 38).

version log:

- 1 2013-11-06
- 2 2013-11-07 inserted lem excerpt
- 3 2014-09-01 outlined introduction structure and appendix key words
- 4 2014-09-11 bibtex included, lem excerpt citet
- 5 2014-09-12 included italic titles in bibliography
- 6 2015-01-12 worked on introduction structure and included magnetic butterfly diagram
- 7 2015-05-04 first printout, small additions
- 8 2015-07-03 coupling functions, content structure
- 9 2015-09-09 Alfvén wave velocity formula
- 10 2015-09-10 Appendix physics: Alfvén and compressional MHD waves, plasma beta; citation sources Cranmer2005, Kivelson1995
- 11 2015-09-15 CGAUSS work overview; DQCS model figure
- 12 2015-09-16 magnetic energy density is the same as magnetic pressure, abbreviations
- 13 2015-09-30 empirical solar wind model plots in analyses, figure label [Figure 4.2 Text]
- 14 2015-10-02 table column decimal alignment; set caption width
- 15 2015-10-05 table units; radial parameter (N, T) profiles in literature
- 16 2015-10-06 literature radial electron density models; log-normal distribution
- 17 2015-10-07 log-normal formulae
- 18 2015-10-08 log-normal fit
- 19 2015-10-09 shape fit parameter table; radial variance fitting
- 20 2015-10-14 variance fit values; log-normal citation Bronstein
- 21 2015-10-19 radial distribution width fitting; clarifying of solar wind model formulae structure and naming variables
- 22 2015-10-20 log-normal distribution width factor changes the shape!
- 23 2015-10-23 log-normal distributions mu and sigma plot
- 24 2015-10-30 new sigmafit2 figures implemented; formulae adaption
- 25 2015-11-02 reason for use of log-normal function
- 26 2015-11-20 single log-normal shape fit; not chisquare - SSR; R^2 in appendix
- 27 2015-11-26 reduced SSR into tables; table column aligning
- 28 2015-12-02 smoothing SSR integration
- 29 2015-12-07 integrating structure remarks from printout

-
- 30 2015-12-09 splitting analyses chapter into two; browsing folders for usable things for thesis
31 2015-12-10 integrating citations and references
32 2015-12-16 integrating citations and references
33 2015-12-18 solar wind structures list of Richardson
34 2016-02-02 sws distributions
35 2016-02-11 basics structure
36 2016-02-12 analyses questions
37 2016-02-15 analyses structure; in situ, near-Sun
38 2016-02-16 Kp index internal resolution
39 2016-02-17 Bartels1962; non-breaking hyphen shorthand implemented
40 2016-02-18 analysesI structure
41 2016-02-25 abstract
42 2016-02-26 english comma
43 2016-03-01 Bartels Kp origin paper, bibtex reference
44 2016-03-02 abstract
45 2016-03-03 Planck paper
46 2016-03-07 formation of stars
47 2016-03-08 formation of stars
48 2016-03-16 solar interior structure
49 2016-03-17 solar interior structure
50 2016-03-18 solar surface
51 2016-03-22 Astronomical Almanac citation
52 2016-03-23 solar core definition
53 2016-03-26 sunspots
54 2016-03-29 Sun interior figure
55 2016-03-30 solar composition
56 2016-03-31 Sun interior figure finished; chromosphere
57 2016-04-01 Sun atmosphere figure finished
58 2016-04-03 chromosphere, corona, CV
59 2016-04-07 CV
60 2016-04-08 CV; heliosphere
61 2016-04-09 corona; heliosphere
62 2016-04-11 heliosheath magnetic bubbles; Opher2011
63 2016-04-12 heliosphere; voyagers; Gurnett2013
64 2016-04-13 solar wind effects, solar rotation
65 2016-04-14 analysesI sws structure draft plots
66 2016-04-15 analysesI concept work
67 2016-04-19 incorporate annotations from processed printout
68 2016-04-21 incorporate annotations from processed printout II
69 2016-04-22 incorporate annotations from processed printout III
69 2016-04-23 updated .bst file (for displaying arXiv id); implemented optional url displaying for electronic version; Kp year variations
70 2016-04-24 Kp frequency by month statistics and plot; Sun and Earth tilt plot
71 2016-04-25 solar cycle extrema dates literature
72 2016-04-27 Kp semi annual variation, Rangarajan1997
73 2016-05-01 Kp frequency by year
74 2016-05-04 Kp + SSN plot; ACE data errors/gaps; log-normal plot; differential rotation plot
75 2016-05-05 aggregate correlation coefficient tables, CME fraction plot
76 2016-05-06 overall sws fractions
77 2016-05-17 figure sw frequencies by year; restructured solar wind distributions section; formal cover page
78 2016-05-20 Earth-Sun distance; JPL web interface
79 2016-05-31 GSM system
80 2016-06-10 Offline Anmerkungen einarbeiten
81 2016-06-12 LaTeX Earth symbol package
82 2016-06-13 numbers=noenddot
83 2016-06-14 references removed comma before ampersand; offline Anmerkungen einarbeiten; thesis_raw version
84 2016-06-17 gnuplot figures and latex; latex document style options
85 2016-06-19 header implemented

86 2016-06-20 minor things; introduction
87 2016-06-23 solar tilt axis
88 2016-06-24 solar rotation
89 2016-07-12 magnetosphere temp figure; analyses: solar wind model
90 2016-07-13 lognormal spelling
91 2016-07-14 constant mass flow rate
92 2016-07-18 line-up periods
93 2016-07-19 line-up periods table
94 2016-07-20 redone line-up analysis
95 2016-07-21 line-up tables
96 2016-07-22 line-up fit function plots; coefficient table
97 2016-07-22 line-up sw types and period plots; overview plot
98 2016-07-24 line-up averaging and justification
99 2016-07-29 line-up rework
100 2016-07-30 line-up structure
101 2016-07-31 line-up table
102 2016-08-02 line-up structure
103 2016-08-03 line-up fits and table
104 2016-08-04 insert offline comments
105 2016-08-15 literature radial sw functions
106 2016-08-18 work offline comments in
107 2016-08-19 work offline comments in
108 2016-08-28 analyses II rework structure
109 2016-08-31 analyses II rework structure
110 2016-09-01 analyses II rework figures
111 2016-09-02 analyses II rework structure
112 2016-09-03 Helios latitude dependency
113 2016-09-04 extrapolation model fit parameter table; Helios latitude dependence
114 2016-09-06 work in offline comments
115 2016-09-14 implement median and mean in composite fit table; create kile project for thesis; url and raw fork
116 2016-09-17 Ulysses polar plot; solar distance plots
117 2016-09-18 for solar distance and latitude -> 4-panel figures created and implemented; appendix figures
118 2016-09-20 latitude plots updated
119 2016-09-26 single lognormal fit figure
120 2016-09-27 minor tweaks in analyses II
121 2016-09-29 simple fit table errors; table style
122 2016-10-05 lognormal fit errors for tables
123 2016-10-10 line-up passing remarks from AP
124 2016-10-12 siunitx package incorporated
125 2017-01-04 package fancyhdr replaced with scrlayer-scrpage; offline comments for Basics + Data incorporated
126 2017-01-06 package floatrow included for figure side captions; some cites; magnetometer
127 2017-01-08 sun figure updates and new ion energy spectrum figure incorporated
128 2017-01-13 offline comments, new chapter order
129 2017-01-18 activated hyperref package; included autoref and eqref; adjusted link colors; header links
130 2017-02-02 offline comments
131 2017-02-03 offline comments II, eclipse image
132 2017-02-06 basics figures with floatrow; flow structure
133 2017-02-07 ion energy spectrum figure
134 2017-02-09 Helios mission ssn plot
135 2017-02-12 offline comments
136 2017-02-13 section number link to toc; offline comments
137 2017-02-14 eclipse and magbfly figure captions
138 2017-02-16 offline comments
139 2017-02-19 coronal heating and sw acceleration
140 2017-04-22 set up git repository
141 2017-04-23 incorporate offline comments

2017-04-23 15:54 – last save

Abstract

This thesis analyzes the solar wind variability, its properties, how they evolve on their way from the Sun and how strong the solar wind's internal structures impact the terrestrial magnetosphere. In situ data from the near-Earth OMNI data set and sunspot number data is used for deriving a functional dependence of the solar wind parameters with the state of the solar cycle. Data from the Helios missions is analyzed and empirical solar wind distance dependencies for 0.3–1.0 au are derived. In view of the planned near-Sun spacecraft mission Solar Probe Plus, additionally the solar wind environment is estimated down to < 10 solar radii. In situ solar wind measurements from the near-Earth OMNI data set are analyzed together with time series of the planetary geomagnetic disturbance indicator K_p . Correlation functions are compiled with regard to forecast the magnitude of the geomagnetic disturbances from solar wind measurements.

Contents

1	Introduction	1
2	Basics	3
2.1	Solar composition	3
2.2	Solar dynamics	6
2.3	Solar wind	9
2.4	Heliospheric magnetic field	9
2.5	Solar wind properties and structures	10
2.5.1	Solar wind plasma	11
2.5.2	Slow solar wind	11
2.5.3	High speed streams	11
2.5.4	Stream interaction regions	11
2.5.5	HCS / HPS	11
2.5.6	Coronal mass ejections	12
2.6	Space weather	12
2.6.1	Solar influence on Earth	12
2.6.2	Magnetosphere	13
2.6.3	Geomagnetic indices	14
2.6.4	Solar wind–magnetosphere coupling	14
3	Data	15
3.1	Instruments	15
3.1.1	Magnetometer	15
3.1.2	Plasma detector	15
3.2	Data sources	16
3.2.1	Sunspot number	16
3.2.2	K _p index	16
3.2.3	OMNI data set	16
3.2.4	Helios probes	17
4	Solar wind time variations	21
4.1	Solar wind variation with solar cycle	21
4.2	Solar wind variation with season	21
4.3	Solar wind empirical forecast	21
5	Solar wind distance variations	23
5.1	Solar wind back-extrapolation	23
6	Helios radial line-up passings	25
7	Solar wind impact on the magnetosphere	31
7.1	Solar wind interaction processes with the magnetosphere	31
7.2	Solar wind–magnetosphere coupling functions	31
7.3	Parameter selection	31
7.4	Data selection	31
7.5	General K _p correlations	32
7.6	Solar cycle influence	32
7.7	Isolating the CME influence	32
7.7.1	Solar wind structure list	32
7.7.2	CME correlations	33
8	Solar wind impact on the terrestrial magnetosphere	35
8.1	Quantifying solar wind impact on the terrestrial magnetosphere	35

8.2	Solar wind structure type influence on the terrestrial magnetosphere	36
8.3	Solar wind structure analyses	37
8.4	CME impact on the magnetosphere	37
8.5	Solar wind frequency distributions	38
8.5.1	Solar wind solar cycle dependence	38
8.5.2	Solar wind seasonal dependence	38
8.6	K _p frequency distribution	39
8.6.1	K _p solar cycle dependence	39
8.6.2	K _p seasonal dependence	40
8.7	Summary/Results	41
8.8	Forecast	41
8.8.1	Internal solar wind correlations	41
8.8.2	K _p forecast from CME velocity	41
8.9	Applications	41
9	Solar wind origin and evolution	43
9.1	Solar wind parameters	43
9.2	Empirical solar wind model	44
9.2.1	Solar distance dependency—theory	45
9.2.2	Solar distance dependency—Helios data	46
9.2.3	Latitude dependency—theory	47
9.2.4	Latitude dependency—Helios data	48
9.2.5	Shape of the frequency distributions	48
9.2.6	Helios solar wind model	51
9.3	Extrapolation model	54
9.3.1	Model validity	55
9.3.2	Model comparison via SSR	55
9.3.3	Adjusted extrapolation models	56
9.3.4	Comparison with existing extrapolation models	56
9.4	Radial evolution of solar wind structures	56
9.5	Summary/Results	57
10	Discussion and results	59
11	Summary and outlook	61
A	Physics	63
A.1	Electromagnetism	63
A.2	Solar wind pressures	63
A.3	Plasma beta	63
A.4	Alfvén waves	64
A.5	Solar surface differential rotation	64
A.6	Earth orbit geometry	65
A.6.1	Solar distance	66
A.6.2	Solar rotation axis tilt	66
A.6.3	Earth tilt	66
A.7	Coordinate systems	66
A.7.1	Geocentric Solar Ecliptic	67
A.7.2	Geocentric Solar Magnetospheric	67
A.7.3	Heliographic Inertial	67
B	Math	69
B.1	Correlations	69
B.2	Lognormal distribution	69
B.3	Goodness of fit	70
B.4	other	71
C	Glossary	73
C.1	Astronomical constants	73

Contents

C.2 Symbols	73
C.3 Abbreviations	73
References	75
Acknowledgments	79
Curriculum vitae	81

1 Introduction

Introductory text -> Motivation for

- time variation analysis
- distance analysis
- K_p impact analysis

Synopsis (chapters, content)

This thesis merges the solar wind analyses of its variation in time (autorefch:), its evolution to Earth (chapter XX) and its impact on the magnetosphere (chapter XX). The solar wind model derived in the first two chapters is used together with SSN predictions to estimate the near-Sun solar wind environment the planned SPP spacecraft will encounter during its mission, beginning in 2018. Lists of constants, symbols and abbreviations used in this thesis are located in the appendix.

2 Basics

First this chapter sketches the Sun's origin, inner structure, atmosphere and heliosphere. Then the Sun's dynamics with its magnetic field variations and solar cycle are outlined (including differential rotation, magnetic field generation, solar cycle, quiet/active Sun characteristics on surface and solar wind with HMF consequences). The solar wind and its characteristic structures are described. Further, the solar influence on Earth, on its magnetosphere and other space weather effects are portrayed.

2.1 Solar composition

13.8 billion years ago the Big Bang formed our universe. The energy density of our universe consists of 69.1 % dark energy, 25.9 % dark matter and 4.9 % baryonic matter according to calculations using the inflationary Λ CDM cosmology together with the latest CMB temperature measurements ([Planck Collaboration et al. 2016](#)). After a few minutes the primordial nucleosynthesis left the universe in a state where the baryonic matter was composed of 75.33 %¹ hydrogen, 24.67 % helium and traces of deuterium, tritium and lithium ([Planck Collaboration et al. 2016](#)).

Over the years this gas cooled down and gravitationally accreted into molecular clouds and formed stars. The first generations of stars (Population III) fused this gas to heavier elements (metals) and supernovae distributed them into space as a foundation for the formation of new stars of low and high metallicity (Population II and I). Likewise, supernovae of these stars constantly enriched the interstellar medium with metals. Now, the interstellar medium in the Milky Way consists of about 32 % helium and traces of other metals ([Danziger 1970](#)).

Our Sun, a metal-rich Population I yellow dwarf star, emerged 4.6 billion years ago ([Bahcall et al. 1995](#)) from an accretion disk formed by a collapsing rotating cloud. The compression within its center resulted in high temperatures which initiated the fusion of hydrogen to helium (primarily pp chain reaction). The fusion reactions produce huge amounts of energy and heat the solar center to a temperature of 15.7 million kelvins ([Christensen-Dalsgaard et al. 1996](#)). The generated energy is transported through the solar body to its surface and eventually into space. The core region extends to about 0.25 solar radii (R_\odot), where the declining temperature becomes insufficient for fusion reactions. The energy transport is dominated by thermal radiation until, because of declining ionization and density, at $0.71 R_\odot$ up to the surface convective motion takes over ([Christensen-Dalsgaard et al. 1991](#)).

The temperature at this transition region (tachocline) is about 2 million kelvins and decreases up to the solar surface to between 4400–6600 K (cite?). Here at the photosphere, the energy is radiated away with an effective black body temperature of 5772 K ([Mamajek et al. 2015](#)), classifying the Sun as a spectral type G2V star. At this surface layer granules, the tops of convection cells, and temporary sunspots are visible. Strong magnetic flux inhibits the convection at sunspots, leading to lower temperature and brightness (for more details on sunspots see the next section 2.2). [Figure 2.1](#) illustrates these photospheric features along with the inner solar structure.

Above the photosphere at the base of the chromosphere the temperature declines to its solar minimum of 3800 K until it raises to 1–3 million kelvins in the corona ([Billings 1959](#)). Up to now it is not fully understood why the corona is so much hotter than the underlying chromosphere—this question is known as the coronal heating problem. The energy transfer mechanisms of choice are magnetic reconnections, wave heating and type II spicules or a combination of these (cite?).

The chromosphere is a 2000 km thick region whose features (numerous spicules, filaments and prominences) can range far into the corona. They consist of by the solar magnetic field channeled chromospheric material, which is enveloped by a thin transition region where the temperature jumps up from ?20 000–35 000 K to coronal temperatures (cite?). Reconnection of magnetic field lines can result in

¹Percentages by mass.

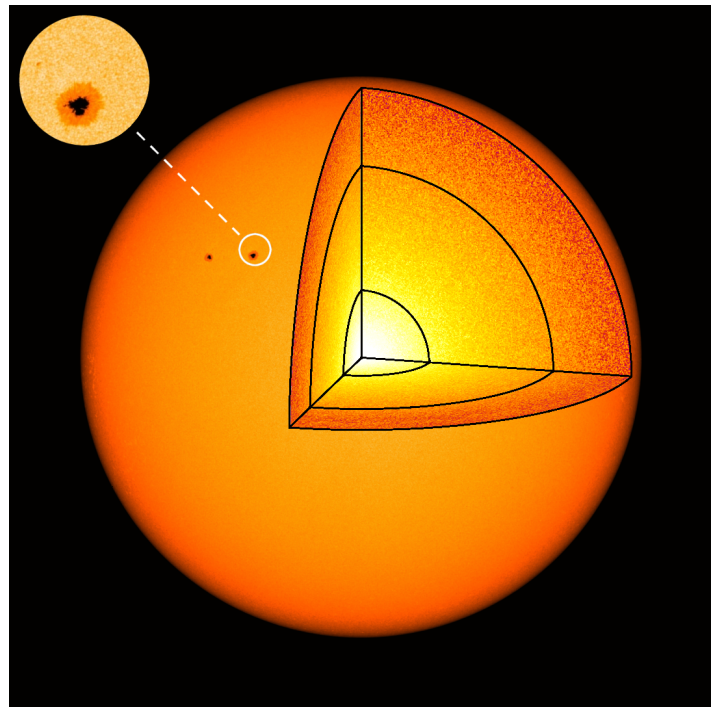


Figure 2.1 Image of the photosphere together with a schema of the solar interior structure. The inset shows the granular surface with a sunspot. The figure is based on a SDO/HMI continuum image from 20 March 2016, credit: NASA/SDO and the AIA, EVE and HMI science teams.

the eruption of filaments into the corona and beyond, termed coronal mass ejections (CMEs) (see also Section XX...). Details of chromospheric features are shown in [Figure 2.2](#).

The Sun's atmosphere is dominated by the varying small- and large-scale solar magnetic field configuration. There are regions where the magnetic field lines arc back to the surface and regions with open field lines. In the latter areas the coronal plasma can—guided by the field—escape into space. Thus these coronal areas are less dense, cooler and therefore appear darker in extreme ultraviolet (EUV) and are called coronal holes (more in Section XX...). In [Figure 2.2](#) a coronal hole is located at the solar south pole.

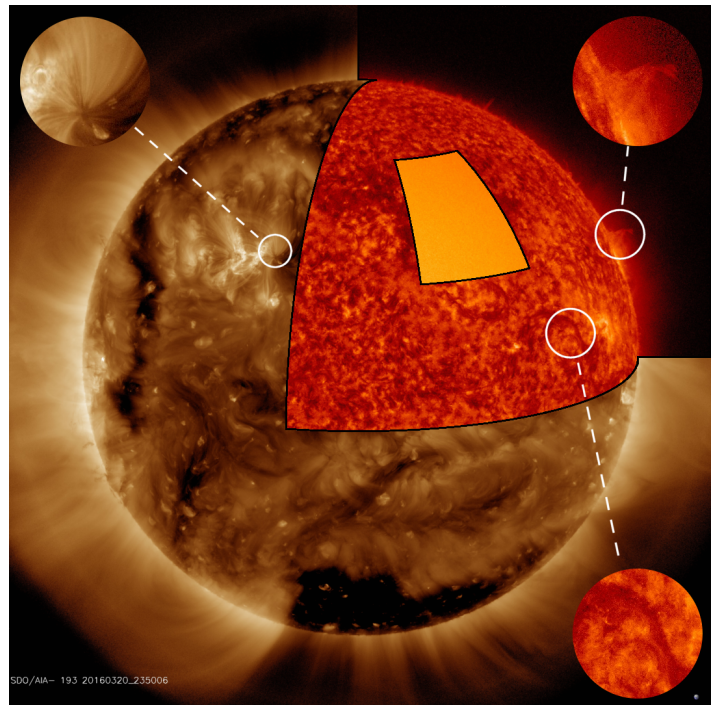


Figure 2.2 Composite image of the solar atmosphere and some of its features. Corona, chromosphere and photosphere are seen in wavelengths of 193 Å, 304 Å and continuum. On the northern limb chromospheric spicules are visible. The enlargements on the right show a prominence and a filament. The dark region at the south pole is a coronal hole. The left inset shows details of the active region belonging to the sunspots in [Figure 2.1](#). The figure is based on SDO/AIA images from 20 March 2016, credit: NASA/SDO and the AIA, EVE and HMI science teams.

From Earth the faint corona and chromosphere can only be observed during eclipses, because of the brightness of the solar disk. There are three effects contributing to the visibility of the corona, photon scattering off free electrons and dust particles, and ion spectral emission lines (termed K-, F-

and E-corona). The image of a solar eclipse reveals the by the magnetic field shaped coronal plasma and features of the red chromosphere, pictured in Figure 2.3.



Figure 2.3 Total solar eclipse image of the inner corona up to 5 solar radii. The picture was taken in Mongolia, 1 August 2008 and is processed from multiple images. Visible are the for a quiet Sun in cycle minimum typical magnetic field's dipole structure and the equatorial streamer belt. Credit: Miloslav Druckmüller, Peter Aniol, Jan Sládeček, 2008. get permission and preferred citation style... into acknowledgments? <http://www.zam.fme.vutbr.cz/~druck/Eclipse/>

Because of the high coronal temperatures, plasma escapes from the solar gravitational field (Parker 1958) with velocities of $200\text{--}800 \text{ km s}^{-1}$. Its acceleration is linked to the coronal heating, but the exact location and process remain an open question (cite?). At a distance of a few solar radii ($\approx 4\text{--}20$) the magnetic field becomes too weak to guide the coronal plasma. From this source surface the solar wind flows radially outward into space until it reaches the termination shock, spanning the heliosphere. Eventually it collides with the local interstellar medium, creating the heliopause. The heliosphere is expected to be a bubble of teardrop shape (and may be led by a bow shock), caused by the Sun's relative velocity of 23 km s^{-1} to the local interstellar medium (Owens & Forsyth 2013). Measurements of the Voyager 1 and 2 spacecraft indicate their passage of the termination shock at about 94 au and 84 au, entering the heliosheath region (Owens & Forsyth 2013). Gurnett et al. (2013) report that in 2012 Voyager 1 actually crossed the heliopause into interstellar space at a solar distance of 121 au. Figure 2.4 illustrates the heliosphere and its surrounding flow structure.

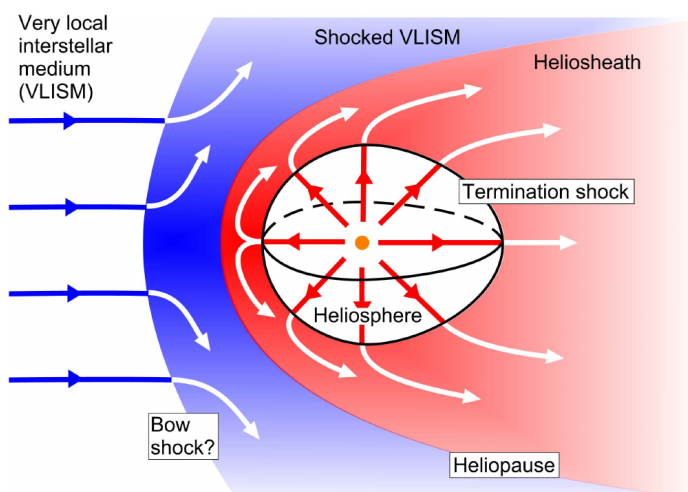


Figure 2.4 Schema of the heliosphere and its surrounding flow structure. The heliosphere is formed by the interaction of the solar wind with the local interstellar medium at the heliopause. (Owens & Forsyth 2013, Fig. 9) get permission...

On its way outwards through the solar system the solar wind, carrying the solar magnetic field, interacts with the planets, their magnetic fields and other solar system bodies. These interactions have various effects, for instance disturbances in planetary magnetic fields with appearance of aurorae and enhanced radiation, atmospheric losses and stripping of cometary tails. Some of these effects can have disruptive consequences for humans and their technology. The topic of space weather effects is further addressed in section 2.6. The magnitude of these effects highly depend on spatial and temporal variations in the solar wind which are rooted in the dynamics of the solar magnetic field.

2.2 Solar dynamics

The spin conservation of the contracting molecular cloud led to a rotation of the Sun with a current average period of about 25 days. The radial convective motion within the solar interior above the tachocline leads to a transport of momentum away from the rotation axis and therefore to a slower polar and faster equatorial rotation in the convection zone (Miesch 2005). This differential rotation is visible on the surface and was first discovered from sunspot observations. With a rotation period of about 34 days the poles have a lag of almost 9 days (for further information on solar rotation see appendix section A.5). The differential rotation in the solar interior can be inferred from helioseismological observations, as seen in Figure 2.5.

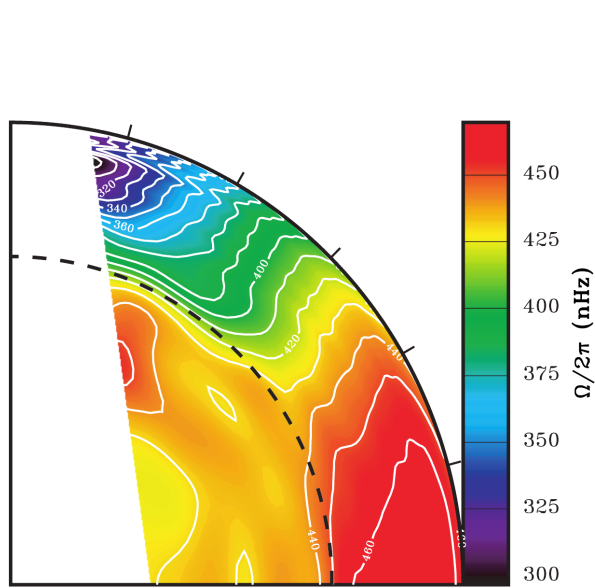


Figure 2.5 Angular rotation velocity in the solar interior. The radiation zone has a nearly solid rotation. Above the tachocline (dashed line) begins the differential rotation of the convection zone. The angular velocity is inferred from helioseismology via observations from the Michelson Doppler Imager (MDI) at the Solar and Heliospheric Observatory (SOHO) spacecraft. (Thompson et al. 2003, Fig. 3) get permission...

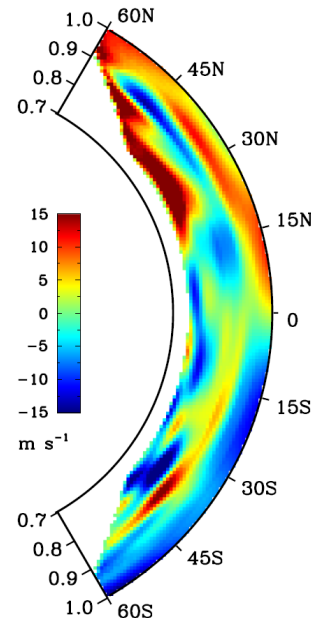


Figure 2.6 Meridional flow velocity profile in part of the convection zone. Positive values are directed towards north. The velocity is inferred from helioseismology via observations from the Helioseismic Magnetic Imager (HMI) at the Solar Dynamics Observatory (SDO) spacecraft. (Zhao et al. 2013, Fig. 4a) get permission...

The resulting large rotational shear at the tachocline generates toroidal magnetic flux (Ω -effect), which convectively raises to the surface forming sunspots. This solar dynamo is thought to create the major part of the solar magnetic field (Miesch 2005).

Helioseismic measurements reveal that the large-scale convective flow is agglomerated into large convection cells with slow meridional flows of a few $m\ s^{-1}$. A poleward subsurface flow and equatorward backflow beneath is detected within each hemisphere, see Figure 2.6.

The cells have a convection cycle of about 22 years (cite...). As the magnetic field is carried by the plasma, it emerges at the surface with the same periodicity. Within one period the surface magnetic field configuration changes from a dipole structure to a reversed dipole structure with opposite polarity, thus the transition time from one dipole state to the next lasts about 11 years.

In the transition phase toroidal magnetic flux emerges in belts above and below the solar equator manifesting as active regions, resulting in a multipolar structured magnetic field.

bipolar active regions are toroidal magnetic flux, which has emerged as a loop from below the pho-

tosphere (magnetic flux ropes).

poloidal field + diff. rot. => toroidal field (Ω -effect) Miesch2005 p. 18 + p. 31
switching between states of strong poloidal and toroidal field

- the solar dynamo: (toroidal to poloidal field)
- turbulent plasma motions from convective flows generate disorganized magnetic fields
- differential shear at tachocline amplifies fields to strong coherent toroidal flux (Ω -effect)
- stronger flux ropes raise to surface (buoyantly)
- Coriolis force twists them systematically, stronger at higher latitudes
- twisted tubes emerge on the surface as bipolar active regions
- amplification of mean fields by fluctuating motions (α -effect) and turbulent diffusion create large-scale poloidal field

Since regions of strong magnetic flux are visible as sunspots on the photosphere, they were known well before the common era by chinese and greek scholars. Systematic sunspot observations exist since 1610, shortly after the invention of the telescope (cite?). In 1843 Schwabe discovered the 11-year periodicity in the sunspot occurrence (cite?). To record solar cycles in 1848 Wolf (et al?) introduced the sunspot number (SSN) and cycle number (with the zeroth occuring in 1749) (cite?), see [Figure 2.7](#). The large variations in cycle length ?(9–14 years) and intensity ?(0–350 S_n) make it difficult to predict

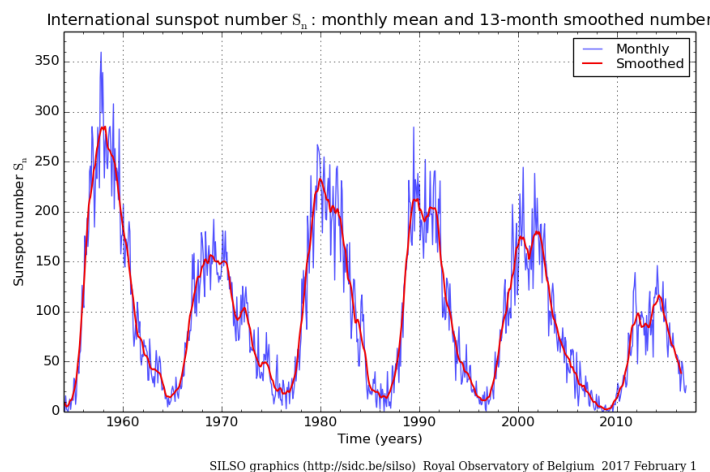


Figure 2.7 Monthly mean sunspot number (blue) and 13-month smoothed monthly sunspot number (red) since 1954. Credit: SILSO data/image, Royal Observatory of Belgium, Brussels, 2017-02-01. get permission... Update this figure before printing!!!

the course of the next solar cycle (cite...).

long-time variations like the Maunder minimum... see Hathaway2015

Observations of the surface radial magnetic field show the appearance of bipolar magnetic flux at belts of about $\pm 20^\circ$ latitude at the beginning of a cycle and a shift towards lower latitudes at the end of a cycle (magnetogram figure of sunspot?). Thus the plot of surface magnetic field over latitude and time reveals a butterfly pattern. The emerging flux (its polarity alternates with each cycle) is carried by the slow meridional surface flow poleward, resulting in the polar field switch, see [Figure 2.8](#). The ordered dipole structure in solar cycle minimum leads to open polar field regions with large coronal holes and a closed equatorial field belt/streamer belt (clearly visible in [Figure 2.3](#)).

sunspot butterfly pattern (Maunder 1904)

sunspots NE active regions; active regions forming streamer belt?

The magnetic field geometry during cycle maximum is more complex, due to the in mid-latitudes emerging flux, which is related to the then stronger toroidal component of the solar magnetic field.

HMF with figures DQCS + Parker spiral

This leads to the chaotic appearance of closed field lines even at higher latitudes/poles and coronal holes covering equatorial regions. tbm

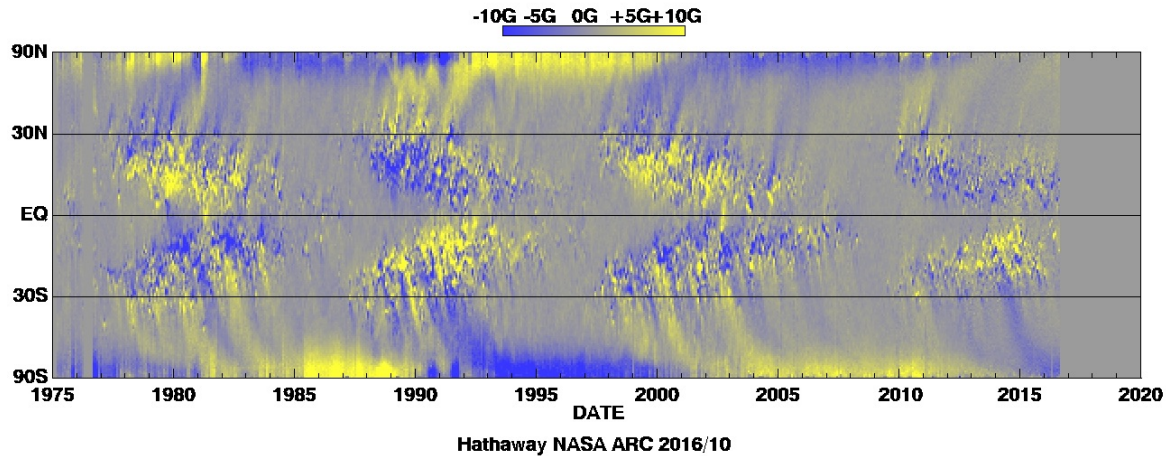


Figure 2.8 This magnetic butterfly diagram maps the synoptic radial magnetic field on the solar surface. Yellow represents an outward directed magnetic field (positive), blue inward (negative). The data is obtained from instruments on Kitt Peak National Observatory and from the MDI at the SOHO spacecraft. Credit: David Hathaway, NASA Marshall Space Flight Center; see also [Hathaway \(2015, Fig. 17\)](#). Update this figure before printing! get permission...

sw in minimum: streamer belt and polar HSSs

fast solar wind emerges from CHs

slow from closed field streamers

This is confirmed by the Ulysses spacecraft, which measured the solar wind speed in a polar orbit covering more than one solar cycle ([Figure 2.9](#)).

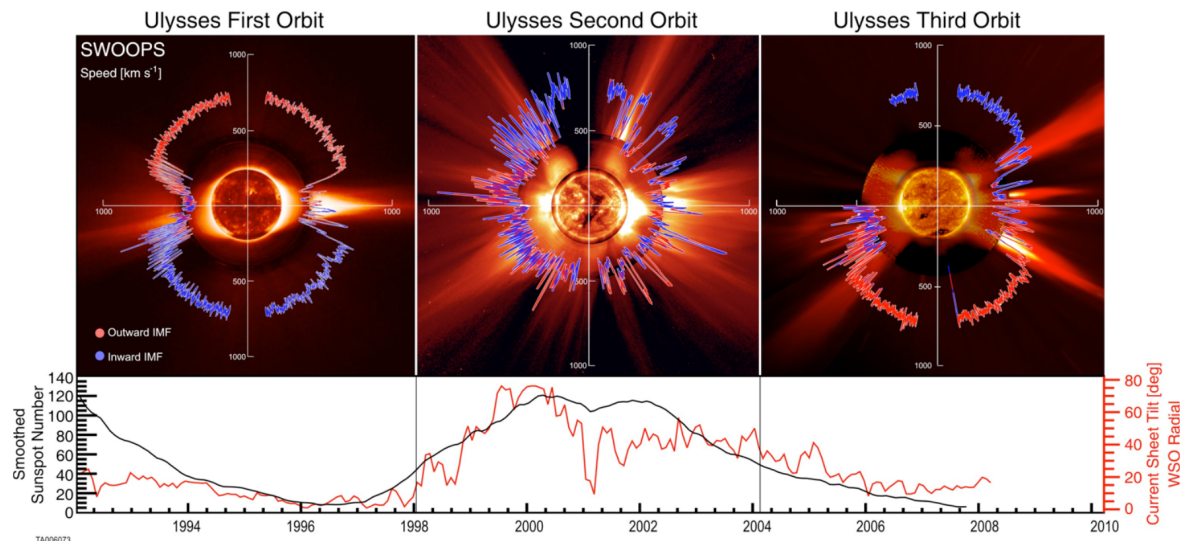


Figure 2.9 Solar wind velocity and magnetic field polarity over latitude during low and high solar activity for the three orbits of the Ulysses spacecraft. The SSN and CS tilt angle are plotted as well. ([McComas et al. 2008, Fig. 1](#)). ask for high res. image and permission...

keywords:

SSN -> magnetic surface activity (butterfly diagram) => poloidal/toroidal field -> min/max polar

CHs (quiet/active Sun figure) -> HMF (quiet B-field figure) -> quiet HMF Parker spiral (figure) -> solar wind -> slow/fast sw pattern (Ulysses figure))

solar wind plasma composition and properties -> visible solar wind structures (coronagraph image; with CME and streamer) -> stream interface (figure) -> in situ measurements (example in situ CIR/HSS plot)

stream interfaces (figure and link to previous CIR plot) -> HCS/HPS

CMEs (link to previous coronagraph image; in situ CME/MC plot; CME schema figure?)

differential rotation/shear at tachocline -> B-field
meridional flow -> solar cycle period
dipole structure, open and closed field lines
polar coronal holes
streamer/equatorial streamer belt
solar wind

open field lines (coronal holes) -> HSSs
equatorial ballerina model -> CIRs (figure?)

The solar differential rotation wraps the magnetic field lines, accumulating tension, leading eventually to relief with a magnetic reconfiguration by field line reconnections.
-> release of much energy -> flares, CMEs

solar wind's impact on Earth

the rotation axis is tilted from the normal of the ecliptic by $i_{\odot} = 7.25^{\circ}$ (U.S. Nautical Almanac Office 2015) (refer to or put into appendix??).

2.3 Solar wind

see Kivelson1995, p14+91

first observed at solar eclipses?, before? deduced by Parker from theory/Carrington from geomagnetic storms?

discovered via eclipses?
see eclipse photo from Druckmüller [Figure 2.3](#)

in 1958 Parker predicted/postulated the solar wind ([Parker 1958](#))
expanding isothermal atmosphere (solar wind model)
continuous supersonic radial outflow of plasma
-> also Parker spiral of HMF (see [Figure 2.11](#))

2.4 Heliospheric magnetic field

reviews: [Balogh & Jokipii \(2009\)](#) (for heliosheath), [Owens & Forsyth \(2013\)](#)

Winterhalter1994 The heliospheric plasma sheet:
"the narrow heliospheric current sheet (ca. 3000–10000 km thick), together with the heliospheric plasma sheet in which it is embedded. The heliospheric plasma sheet region is identified by a significantly enhanced plasma beta caused by density enhancements and diminished magnetic field strength and is about 20 to 30 times the thickness of the current sheet."
heliospheric current sheet (HCS)
heliospheric plasma sheet (HPS)

ballerina model... (search figure...)

Photosphere: magnetic bright points (MBP) 1–2 kG
 their convective motion result in wavelike fluctuations of the thin tubes
 low chromosphere: thin flux tubes expand laterally and merge to a homogeneous network field
 below the chromosphere-corona transition region: the network magnetic field expands laterally and merges again to a large-scale canopy (image)

[above the Alfvén critical point—where the wind speed equals the local Alfvén speed at about $10 R_\odot$ —both the inward and outward modes are advected (advection: convect horizontally) outward with the wind
 superradially expanding magnetic flux tube
 (Cranmer & van Ballegooijen 2005)]
 see also paper citations...

analytical solar magnetic field model for solar minimum conditions (Banaszkiewicz et al. 1998)
 dipole plus quadrupole plus current sheet (DQCS) solar magnetic field model
 The DQCS model with its quadrupole part having a direct link from the solar equator to infinity along the equatorial plane and current sheet. (see Figure 2.10) (Banaszkiewicz et al. 1998)
 compare with field geometry from eclipse Figure 2.3...

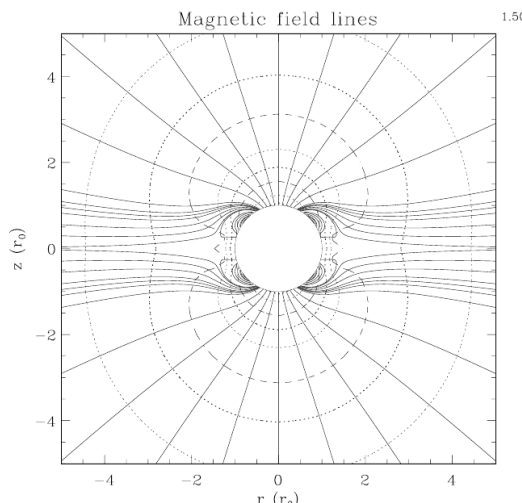


Figure 2.10 Solar magnetic field geometry from the DQCS model with field lines (solid) and constant field strength surfaces (dashed). The quadrupole part allows equatorial outflows along the current sheet. (Banaszkiewicz et al. 1998, Fig. 3) get permission...

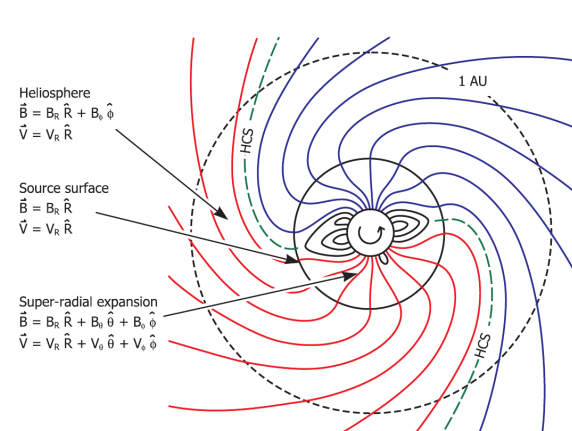


Figure 2.11 Illustration of the solar magnetic field Parker spiral formation by rotation of the solar wind source surface. Between solar wind flows of opposite magnetic field polarity a heliospheric current sheet (HCS) forms. (Owens & Forsyth (2013, Fig. 1), adapted from Schatten et al. (1969, Fig. 1)) get permission...

Parker spiral, source surface and HCS, see Figure 2.11

MHD simulations based on Voyager 1 and 2 measurements within the heliosheath indicate the formation of magnetic bubbles (reconnected sector regions) at the sector boundary caused by the compression before the heliopause, flowing away to the heliosheath tail (Opher et al. 2011).

2.5 Solar wind properties and structures

list event/structure types

solar wind structures source regions: sunspots/active regions, coronal holes, filaments

2.5.1 Solar wind plasma

Plasma in general (properties (H/He/metal composition; see paper...), Plasma-beta, etc.)
solar wind properties, slow/fast wind, MHD waves (Alfvén waves)

special events/configurations, which can appear (CIRs, HCS/HPS, etc.) HSS, sector boundaries, CIRs, CMEs

2.5.2 Slow solar wind

regions with closed lines
trapped plasma, slow solar wind from streamers

2.5.3 High speed streams

regions with open lines
coronal holes as sources of fast sw

sw plot of HSS with CIR to refer to

[Schwenn \(1983\)](#): “During the Skylab era in 1973/74 we learned that these high speed streams emerge from coronal holes (Hundhausen, 1977 and references therein).”

2.5.4 Stream interaction regions

Streams of fast wind catch slow wind
-> compressions, shocks, deflections

Corotating interaction regions (CIRs)
Stream interaction regions (SIRs)

formation of stream interface and stream deflection, see [Figure 2.12](#)
refer to sw figure of CIR

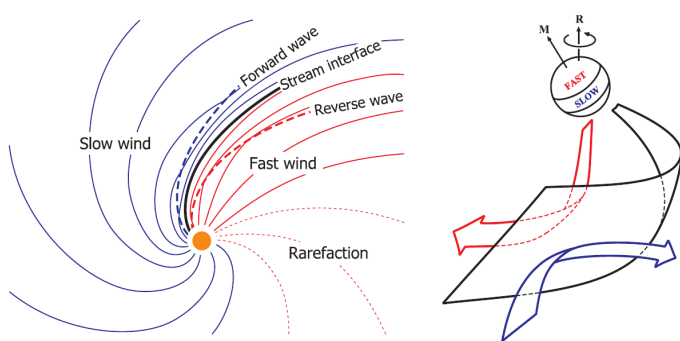


Figure 2.12 Schema of the formation of a stream interface (left) and deflection of streams (right), both generated from interactions between slow and fast solar wind. ([Owens & Forsyth \(2013, Fig. 7\)](#); right panel adapted from [Pizzo \(1991, Fig. 2\)](#)) get permission...

2.5.5 HCS / HPS

from sector boundaries (ballerina skirt)

2.5.6 Coronal mass ejections

Coronal mass ejections (CMEs) (discovery (Carrington), definition (Hundhausen?), models, GCS (conception of 3-dim CME shape -> enables Earth arrival time forecast from modeled direction and velocity))

active regions:
sunspots, magnetic reconnections, flares, post-eruptive arcades

coronagraph figure of CME (COR2 image, SECCHI/STEREO)
in situ solar wind figure of same CME (recent one from 2016)

CME-plasma properties
+ flares and SEPs often accompany CMEs

Magnetic clouds

magnetic cloud (MC); refer to in situ plot
See BS magnetic cloud model in analyses methods chapter MVA...

2.6 Space weather

Solar wind influences the Earth's magnetosphere and can disturb sensitive technical systems
understanding its properties helps with prediction of events

influences on human infrastructure/technical systems

various space weather effects, for instance disturbances in magnetic fields, aurorae, episodes of enhanced radiation, atmospheric losses and stripping of cometary tails. figures of these effects?

reference to [Bothmer & Daglis \(2007\)](#), maybe images

2.6.1 Solar influence on Earth

Carrington made first connection between terrestrial magnetic field and solar flares. correct?

there are several types of solar-terrestrial relations, [Bartels \(1962\)](#) listed:
a) irregular flare and CME effects (Carrington)
b) 11-year solar cycle effects
c) 27-day solar rotation effects
d) daily effects (x-ray and light)

seasonal effects from Earth orbital distance, inclination (solar rotation axis angle) and Earth tilt
(get figure...)

solar wind and its species
solar radiation
solar energetic particles (SEPs)
gravitation

magnetosphere
ionosphere?
aurorae
geomagnetic storms (several days, from CMEs)
substorms (few hours, from CIRs??)

for humans and their technology important effects: enhanced radiation, geomagnetic storms
lovely, disruptive, dangerous consequences <- read in VBbook

at Earth the solar wind total energy flux (1.45 mW/m^2) is only about one millionth of the solar radiation flux (see Schwenn (1990, p. 153))

2.6.2 Magnetosphere

shape formed by dynamic pressure..., similar to heliosphere in ISM...

bow shock, magnetotail, magnetosheath, magnetopause
add ecliptic and terrestrial tilt angle; with plasmoid?
see Figure 2.13

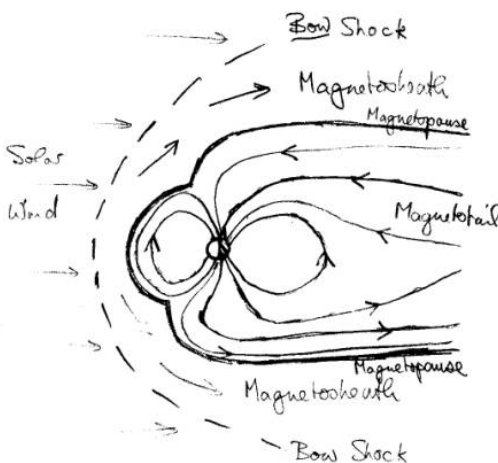


Figure 2.13 temp figure “The cavity is called the magnetosphere. It has a relatively well-defined outer boundary, the magnetopause.”

turbulence with sw (KH or RT instabilities), see subsection 2.6.4

Earth magnetic field strength at a height of 36 000 km (geostationary): 100 nT
Earth magnetic field strength at the surface - equator: 30 000 nT - poles: 60 000 nT (cite?)

magnetopause = current layer??

two extreme cases of B_z orientation: parallel/antiparallel compression/reconnection (with figure)

standoff distance: (Bothmer & Daglis 2007, p. 112)

$$d = \frac{107.4}{1R_E}(NV^2)^{-1/6} \quad (2.1)$$

Even in “ancient” times (when?) a correlation between solar particles and disturbances in the magnetosphere were known of (Bartels1962).

magnetosphere variations due to solar wind
magnetosphere protects from radiation (maybe from solar wind stripping atmosphere away?)

effects: aurorae, ...

ring current systems

definition of:
magnetic storm...

2. Basics

substorm...

subsection Ionosphere?
its variations due to solar radiation (day/night cycle and flares)
ionosphere -> TEC -> GNSS error

2.6.3 Geomagnetic indices

for Kp, AA and Dst read Section 7.4 in book [Bothmer & Daglis \(2007\)](#)...
Geomagnetic indices (variety of indices AA, AE, Dst, etc.)
Kp index, construction from 13 K stations... (-> look into early presentations)
The Kp index is described in [subsection 3.2.2](#).

AE - intensity of northern polar electrojet
Dst - intensity of magnetospheric ring current
Ring-Current Index Dst (read book Jursa1985 p. 4-31)

2.6.4 Solar wind–magnetosphere coupling

E-field:

$$\mathbf{E}_{\text{IMF}}? = -\mathbf{V} \times \mathbf{B}_{\text{IMF}} \quad (2.2)$$

...derive from Lorentz force
(Because of high plasma conductivity the E-field is not existent.)

Axford1964 viscous interaction (of turbulent nature, KH/RT instabilities, KH instabilities at the flanks of the magnetosphere) is a viable source of drag force/solar storm energy input into magnetosphere

Otto&Nykyri1982 KH instabilities/vortices force magnetic reconnection even at northern IMF and are able to account for observed mass flux

[Newell et al. \(2007\)](#) and [Newell et al. \(2008\)](#): coupling consists of merging and viscous part (reconnection and turbulence)
merging part: rate magnetic flux is opened at the magnetopause
viscous part: reconnection due to Kelvin-Helmholtz instabilities at the boundary

Merkin2013 MHD simulation of velocity shear at magnetosphere boundary with northern IMF; KH instabilities; double-vortex sheet structure

3 Data

3.1 Instruments

For analyzing the solar wind and related effects on the Sun there are remote instruments (solar imager and coronagraphs) and in situ instruments (magnetometer and plasma detector).

Here the basic principles of the latter are described, because the analyses performed in this thesis are based on in situ solar wind measurements.

3.1.1 Magnetometer

Spacecraft nowadays carry two different magnetometer types, one for measuring the magnetic field direction and its strength and the other for observing the magnetic flux and detecting waves.

A flux gate magnetometer consists of two coils around a core—one coil with alternating current, which is compared with the induced current signal from the other. Without external magnetic field both patterns match. The core is easier magnetized in direction of an existing external magnetic field, in which case the patterns differ. It measures...

In a search coil magnetometer one coil is placed around a core; measures plasma waves - where?

Because these magnetometer types are directional, they often are placed in two sets of triaxial configurations, attached on booms to minimize the influence of the spacecraft's own magnetic field.
L-> which is generated by surface charges?/electrons?/ionization?/the instruments?

3.1.2 Plasma detector

several spectrometers with different energy ranges

isotope spectrometer - isotopic abundances of SEPs
ionic charge analyzer - charge state of SEPs
sw ion mass spectrometer -
sw ion composition spectrometer -
radio burst tracker

A plasma detector measures the ion energy frequency distribution, which consists basically only of protons and alphas in solar wind (see Figure 3.1). see also subsection 2.5.1

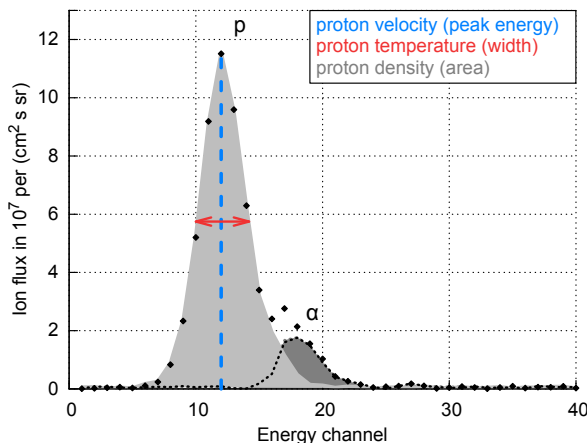


Figure 3.1 Example of an ion energy spectrum with synthetic data. Here proton and helium (alpha) peaks are distinguishable...

3. Data

From the energy spectrum the velocity, density and temperature can be derived.

The bulk velocity is derived from the distribution's average energy.
The number density is the area of the distribution.
The temperature scales with the distribution's width.

3.2 Data sources

Spacecraft / data sets

Positions:
Earth:
imager, magnetosphere
L1 - Lagrangian point:
ACE (siehe auch space weather spacecraft Liste)
Wind etc. (OMNI)
inner heliosphere:
Helios 1 & 2
outer heliosphere:
Voyager 1 and 2
Ulysses

also RT-data sources?

3.2.1 Sunspot number

SSN history
add SSN figure of history incl. Maunder minimum?

SIDC/SILSO...
WDC-SILSO – World Data Center-Sunspot Index and Long-term Solar Observations

3.2.2 Kp index

Kp index first introduced by [Bartels & Veldkamp \(1949\)](#)
it was maintained at the University of Göttingen...

insert figure of Kp musical diagram

mention IAGA...

The German Research Centre for Geosciences (GFZ) in Potsdam supplies indices of global geomagnetic activity, more precisely the Kp index and thereof derived indices. The GFZ provides historical and quicklook data of the indices via their website¹.

list Kp derived indices
ap, Ap, K, Cp, ...

3.2.3 OMNI data set

a data set merged from different sources
The OMNI data ([King & Papitashvili 2005](#)) were obtained from the GSFC/SPDF OMNIWeb interface.

¹GFZ website: <http://www.gfz-potsdam.de/sektion/erdmagnetfeld/daten-produkte-dienste/kp-index/> (existent in 2017-02-12)

from spacecraft located near the Lagrange point L1 upstream of Earth time-shifted to the bow shock of the magnetosphere

OMNI2 H0 MRG1HR (1963-201308) Cite from CDAweb: Hourly near-Earth solar wind magnetic field and plasma data, energetic proton fluxes (> 1 to > 60 MeV), and geomagnetic and solar activity indices.

- NASA, Goddard Space Flight Center (GSFC), Space Physics Data Facility (SPDF): <http://spdf.gsfc.nasa.gov/>
- Coordinated Data Analysis Web (CDAWeb): <http://cdaweb.gsfc.nasa.gov/>
- OMNIWeb Plus: <http://omniweb.gsfc.nasa.gov/>

OMNI spacecraft data coverage (see also talk 2014-02-18)
see Figure 3.2

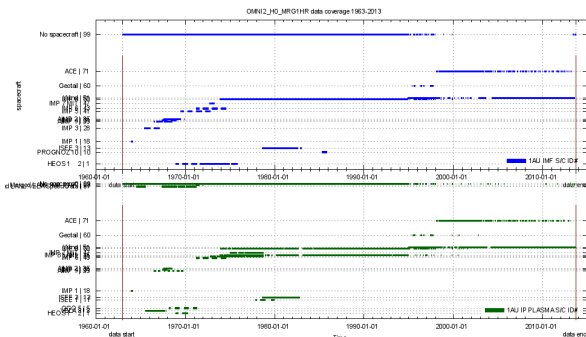


Figure 3.2 OMNI intercalibrated multi-spacecraft data coverage per spacecraft. renew plot until 2016-12-31; integrate into 1 panel...

Advanced Composition Explorer

s/c figure, launch date was 25 August 1997

MAG – fluxgate magnetometer
SWEPAM

data errors/gaps...

DSCOVR as replacement was launched on 11 Februar 2015. It is NOAA's SWPC real-time solar wind prime source since 27 July 2016.²

Solar Wind Structures

Solar Wind Structures (SWS) list
derived by Richardson.... from OMNI data (only?)
permission received.

characterization of near-Earth solar wind structures since 1963
SWS lists (Richardson et al. 2000) and (Richardson & Cane 2012)

3.2.4 Helios probes

see Helios data readme.txt
see paper

two different fluxgate magnetometers and a search coil magnetometer

see Figure 3.3

²<http://www.swpc.noaa.gov/products/real-time-solar-wind>

3. Data

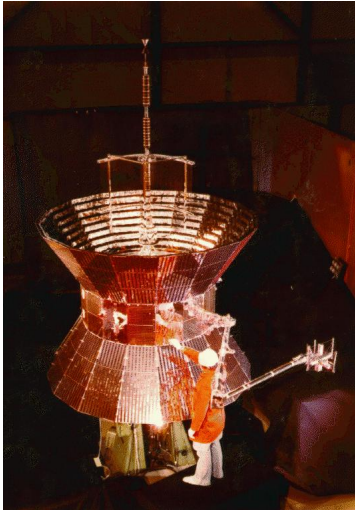


Figure 3.3 One of the nearly identical twin Helios spacecraft. Credit: Max Planck Institute for Solar System Research. get permission...

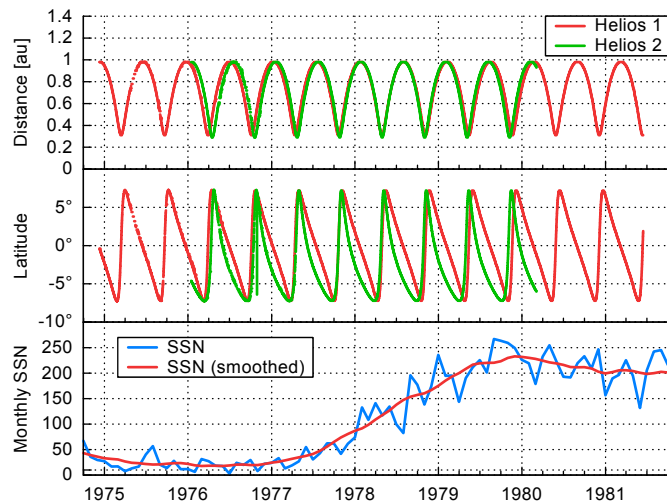


Figure 3.4 Plot of the Helios probes' solar distance and HGI latitude over their mission time, together with the monthly SSN and 13-month smoothed monthly SSN.

solar distance, HGI latitude and sunspot number during the Helios missions; see [Figure 3.4](#)

Helios orbit in the ecliptic plane (see [Figure 3.5](#)) and in the latitude polar plane (see [Figure 3.6](#)); make 2-panel figure...

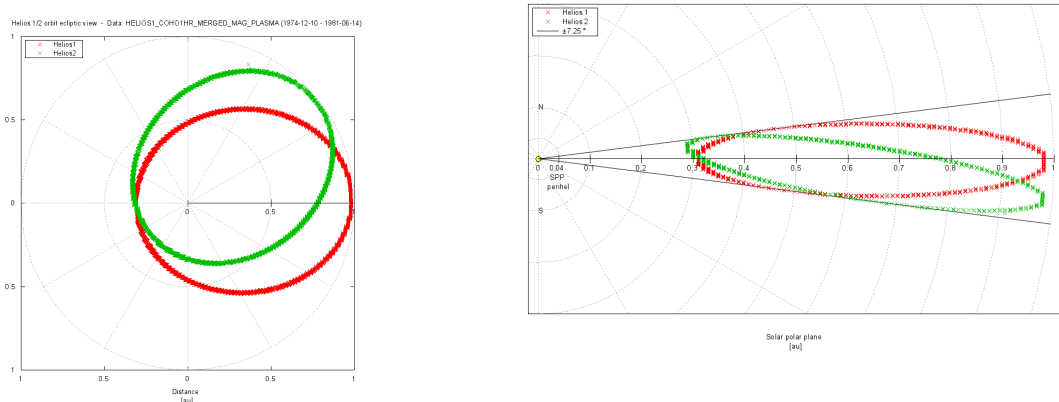


Figure 3.5 Plot of the Helios orbits in the ecliptic plane (left) and polar plane (right) (in HGI-coordinates). combine with polar plane plot...

Figure 3.6 combine with other plot...

The Helios magnetic field and plasma data counts over solar distance are plotted in [Figure 3.7](#) and over latitude are plotted in [Figure 3.8](#). build 2-panel figure...

Solar wind data courtesy of R. Schwenn, Max-Planck-Institut für Aeronomie, Lindau, magnetic field data courtesy of F. Neubauer, Universität zu Köln. (see paper; into acknowledgements...)

data sources – see paper for replacing the following data
 solar wind parameters: ACE, Helios, OMNI
 geomagnetic indices: K_p, OMNI

Space Physics Data Facility (SPDF)

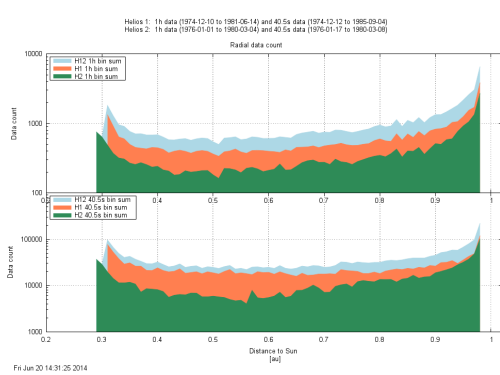


Figure 3.7 Plot of the Helios data count per 0.01 au solar distance bins. plot for mag and plasma individually..., combine with latitude plot...

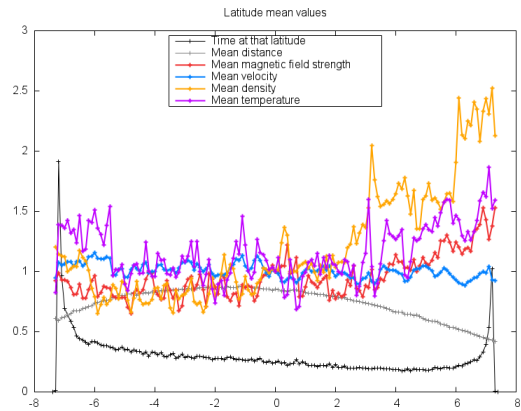


Figure 3.8 Plot of the Helios data count per 0.1° latitude. plot for mag and plasma individually... remove all other curves...

HELIOS 1 and 2 - orbital Parameters

<http://spdf.sci.gsfc.nasa.gov/pub/data/helios/helios1/traj/>
<http://spdf.sci.gsfc.nasa.gov/pub/data/helios/helios2/traj/>

Helios hourly merged mag & plasma data:

HELIOS1_COHO1HR_MERGED_MAG_PLASMA_2965.txt
 HELIOS2_COHO1HR_MERGED_MAG_PLASMA_3096.txt

<http://cdaweb.gsfc.nasa.gov>

temporal coverage of merged data

Helios 1: 1974-12-10 - 1981-06-14

Mag data availability: 42.6 %

Plasma & orbit data availability: 76.4 %

Helios 2: 1976-01-01 - 1980-03-04

Mag data availability: 54.4 %

Plasma & orbit data availability: 91.8 %

4 Solar wind time variations

- 4.1 Solar wind variation with solar cycle**
- 4.2 Solar wind variation with season**
- 4.3 Solar wind empirical forecast**

5 Solar wind distance variations

5.1 Solar wind back-extrapolation

see paper...

McGregor2011 analyzed the empirical magnetic topology–velocity relationship, using Helios perihelion data with the Wang-Sheeley-Arge (WSA) coronal model, and found indications, that the fast and slow solar wind are generated from distinct sources. (not only superradial expansion)

6 Helios radial line-up passings

have a look into Schwenn1984...

To derive the radial dependence of the solar wind parameters directly, we look at the passings when both Helios spacecraft were radially lined up. In these cases they flew through the same solar wind at different solar distances.

(This eliminates the bias of averaging over slow and fast wind streams, like the described model does.) see also [Schwenn \(1990\)](#) p. 156 + p. 122...

we compare these independently derived radial fit functions to those obtained from the averaging over all solar wind types...

There were eight passings when both Helios spacecraft were radially lined-up (see [Figure 6.1](#)). These points in time, when both probes had no separation in heliographic longitude, are derived from

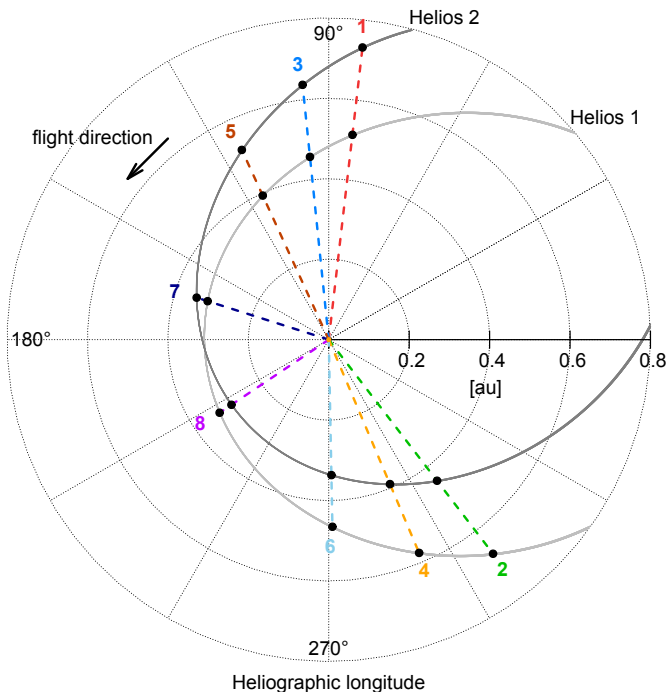


Figure 6.1 Schema of the eight spacecraft line-up positions of both Helios probes on their respective orbits. make B&W... combine with fig 5.15? calibrate text size

Helios 1 and Helios 2 daily trajectory data (for the data source see Section XX). The data is linear interpolated to get an hourly resolution. The resulting points in time together with solar distances are listed in [Table 6.1](#).

The last two passings were merely one week apart and the Helios probes flew almost without radial separation because Helios 2 overtook Helios 1 during its perihelion. As we want to analyze the same solar wind at different solar distances, we exclude the passings 7 and 8 from further analyses.

The passing longitude is not the same as the longitude where the solar wind is detected by both spacecraft consecutively. A passing occurs shortly before the points in time when both spacecraft observe the same solar wind. For the outer probe this point in time is shifted by the solar wind's travel time. The travel time depends on the solar wind's velocity and its distance traveled.

6. Helios radial line-up passings

Table 6.1 Times when both Helios probes had no separation in heliographic longitude. Their solar distances (inner spacecraft r_1 , outer spacecraft r_2) were in the range 0.291–0.731 au and the maximal inter-probe radial distance dr was 0.229 au. errors in au...

Passing	Date	Time	Inner s/c	r_1 [au]	r_2 [au]	dr [au]
1	1976-03-09	00:00	Helios 1	0.513	0.731	0.219
2	1976-05-02	14:00	Helios 2	0.442	0.671	0.229
3	1976-09-19	10:00	Helios 1	0.457	0.637	0.180
4	1976-10-31	11:00	Helios 2	0.390	0.576	0.186
5	1977-04-02	12:00	Helios 1	0.394	0.519	0.125
6	1977-04-30	23:00	Helios 2	0.337	0.465	0.128
7	1977-10-18	06:00	Helios 1	0.316	0.345	0.029
8	1977-10-25	19:00	Helios 2	0.291	0.327	0.035

Based on the obtained spacecraft line-up time t_0 one can calculate the offset times t_1 and t_2 when the inner and outer spacecraft pass by the same solar wind (see Figure 6.2). At the solar wind line-up longitude the condition

$$t_2 = t_1 + t_{sw} \quad (6.1)$$

holds. As the offset times depend on the solar wind travel time between the probes, we need knowledge of the solar wind velocity v for their calculation: $t_{sw} = dr/v$, with the mean radial separation distance dr between the probes.

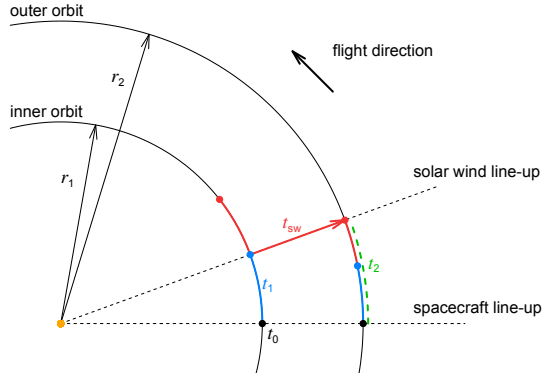


Figure 6.2 Illustration of the solar wind line-up longitude situation with the spacecraft line-up time t_0 , the offset times t_1 , t_2 (at which the spacecraft measure the same solar wind) and the solar wind travel time t_{sw} . combine with fig 5.14?

For the calculation of t_1 we recall the third Kepler law

$$\frac{T_1^2}{T_2^2} = \frac{a_1^3}{a_2^3} \quad (6.2)$$

with the orbital periods T_1 , T_2 and the semi-major axes a_1 , a_2 . The assumption of circular orbits (why? what error size?) leads to

$$\begin{aligned} \frac{t_1^2}{(t_1 + t_{sw})^2} &= \frac{r_1^3}{r_2^3} \\ \Leftrightarrow \quad t_1 &= t_{sw} \left(\left(\frac{r_1}{r_2} \right)^{\frac{3}{2}} - 1 \right)^{-1} \end{aligned} \quad (6.3)$$

and finally the offset time t_1 only depends on the variable solar wind travel time t_{sw} .

Due to uncertainties in the travel time t_{sw} (the solar wind speed v is obviously not a constant) the exact calculation of t_1 is imprecise. To get a reliable result we perform two iterations calculating the offset time from the average velocity \bar{v} of the surrounding 2-day period. We use the velocity \bar{v}_0 around t_0 to calculate the offset time t'_1 as a first estimate. As the velocity \bar{v}'_1 at t'_1 is certainly different, we use this velocity to refine the value and obtain t_1 . Hence deriving the velocity \bar{v}_1 enables us to calculate the solar wind travel time t_{sw} .

The average velocities are obtained from the hourly merged (mag?) and (plasma?) Helios data set (see Section XX). The resulting offset times and velocities of both iterations together with the travel times are listed in [Table 6.2](#).

Table 6.2 The two iterations of the derived offset times and average velocities. The resulting solar wind travel times have durations of 11–28 hours. errors...

Passing	Inner s/c	v_0 [km/s]	t'_1 [h]	v'_1 [km/s]	t_1 [h]	v_1 [km/s]	t_{sw} [h]
1	Helios 1	659.3	19.6	656.9	19.7	656.9	13.9
2	Helios 2	436.4	25.1	370.9	29.5	356.7	26.7
3	Helios 1	482.6	24.0	444.0	26.1	413.8	18.1
4	Helios 2	302.3	32.2	279.9	34.8	278.3	27.8
5	Helios 1	507.3	20.0	474.8	21.4	473.5	11.0
6	Helios 2	321.2	26.6	392.6	21.7	367.8	14.5

For the solar wind line-up longitude condition ([6.1](#)) holds. For all other positions the solar wind measured by the inner spacecraft will not arrive the outer orbit position at the same time as the outer spacecraft does (see [Figure 6.3](#)).

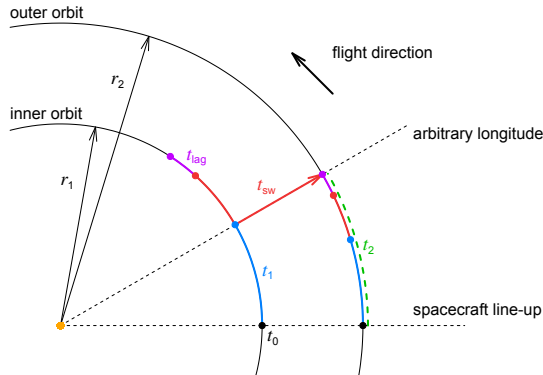


Figure 6.3 Illustration like [Figure 6.2](#) but for arbitrary longitude situations a lag time t_{lag} comes into play. merge with fig 5.14?

Either the spacecraft (negative lag time) or the solar wind (positive lag time) already have passed this position:

$$t_2 = t_1 + t_{\text{sw}} + t_{\text{lag}}. \quad (6.4)$$

This lag time t_{lag} is the time difference at which the solar wind is probed by both spacecraft. At the spacecraft line-up longitude ($t_1 = t_2 = 0$) the lag time equals the solar wind travel time and at the solar wind line-up longitude the lag time is zero.

We choose to look at time periods (instead of points in time) around the offset times to derive average solar wind parameters. This helps reducing the influence of solar wind fluctuations.

We define the period duration boundaries as when the lag time t_{lag} is in the range ± 24 h. For the outer spacecraft these periods are almost twice as long as for the inner spacecraft. The calculated period start and end hours (relative to t_0) for both spacecraft are listed in [Table 6.3](#) together with the data coverage of these periods.

6. Helios radial line-up passings

Table 6.3 Derived period start and end hours for both spacecraft in relation to the longitude line-up time t_0 . The corresponding combined data coverage within that period of the magnetic field, velocity, density and temperature is listed as well. instead duration! errors...

Period	s/c	Inner spacecraft			Outer spacecraft		
		Start [h]	End [h]	Coverage [%]	Start [h]	End [h]	Coverage [%]
1	Helios 1	-14.4	53.8	73	-24.6	91.6	99
2	Helios 2	3.1	58.3	89	5.8	109.0	88
3	Helios 1	-9.2	65.1	16	-15.1	107.2	10
4	Helios 2	4.8	65.2	59	8.5	117.0	87
5	Helios 1	-25.5	68.3	89	-38.5	103.3	88
6	Helios 2	-15.3	61.7	93	-24.8	100.1	92

For period 3 the combined data coverage of the four solar wind parameters is only 16 % (Helios 1) and 10 % (Helios 2) respectively. We consider this as insufficient for the continuing analysis and therefore also omit period 3.

The five remaining periods are marked in [Figure 6.4](#).

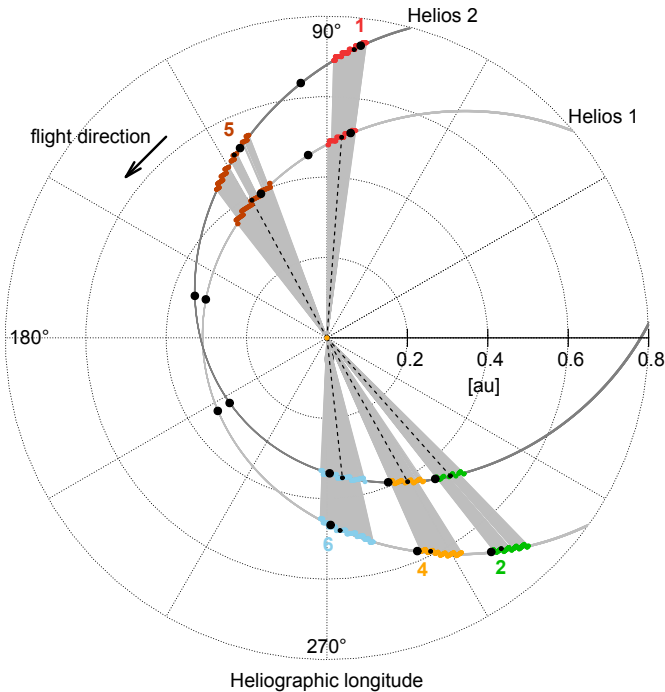


Figure 6.4 Scheme of the line-up periods of both Helios spacecraft on their respective orbits. The corresponding orbit sections which we consider in our analysis are marked in color. These sections span the positions where both spacecraft observed the same solar wind with a maximal lag time of ± 24 hours. bw figure?? dotted lines?

The average values of the four parameters magnetic field B , velocity v , density n and temperature T are listed in [Table 6.4](#).

If we compare both, the inner solar wind sections together with their outer counterparts, they indeed appear to have a similar shape apart from the time shift (see [Figure 6.5](#)) (name definite features...). This confirms that they indeed are parts of the same solar wind structures.
maybe figures of all into Appendix?...

the comparison to the sw model's mean value at the individual distances lets us classify the solar wind types...

Period 1 HSS

Table 6.4 Average values of the four solar wind parameters magnetic field, velocity, density and temperature for the individual periods and spacecraft. errors...

Period	s/c	Inner spacecraft				Outer spacecraft			
		B [nT]	v [km/s]	n [cm ⁻³]	T [K]	B [nT]	v [km/s]	n [cm ⁻³]	T [K]
1	Helios 1	17.04	646.4	12.0	367 300	8.93	602.8	6.7	244 000
2	Helios 2	15.77	356.4	38.8	122 400	12.05	390.2	17.7	117 200
4	Helios 2	15.18	281.3	108.0	46 000	10.64	298.6	46.1	30 400
5	Helios 1	28.80	521.3	45.9	337 800	18.73	530.3	24.4	282 000
6	Helios 2	29.57	402.4	82.5	271 900	14.71	432.6	35.7	199 100

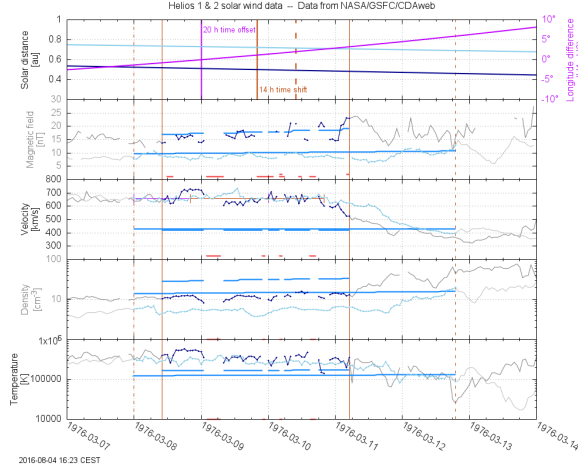


Figure 6.5 Measured solar wind parameters B , v , n , and T of both spacecraft in the period 1. Also plotted is the spacecraft's separation in heliographic longitude. offset time, time shift; expected value from the radial sw model... remove date... remove solar distance... adjust text size...

Period 2 medium-LSS

Period 4 LSS

Period 5 medium-HSS

Period 6 LSS-HSS

We obtained the mean parameter values for the inner and outer solar wind sections. As with the overall radial dependency before, these two points are fitted to the exponential regression fit function $X(r) = X_0 r^{cx}$ (see Section XX. The resulting fit coefficients for each period are listed in **Table 6.5**. why is it better to fit the period's mean values than the whole period?... we fit the periods' mean value rather than the whole periods, because...

Table 6.5 Radial fit functions $B(r)$, $v(r)$, $n(r)$ and $T(r)$ for each period. or only the variables into table? error sizes...

Period	$B(r) = B_0 r^{cb}$ [nT]	$v(r) = v_0 r^{cv}$ [km/s]	$n(r) = n_0 r^{cn}$ [cm ⁻³]	$T(r) = T_0 r^{ct}$ [K]
1		$4.88 r^{-1.815}$	$564.7 r^{-0.196}$	$3.9 r^{-1.647}$
2		$9.50 r^{-0.654}$	$442.6 r^{0.220}$	$8.9 r^{-1.902}$
4		$6.79 r^{-0.900}$	$322.0 r^{0.151}$	$15.7 r^{-2.155}$
5		$5.99 r^{-1.649}$	$554.8 r^{0.065}$	$4.6 r^{-2.423}$
6		$3.22 r^{-2.108}$	$506.5 r^{0.219}$	$5.7 r^{-2.533}$
weighted by duration mean functions				
mean of sw model (update)		$6.078 r^{-1.563}$	$435.5 r^{0.04955}$	$7.613 r^{-2.032}$
				$97\,050 r^{-0.8002}$

The fit curves show noticeable deviations from the model's mean fit (see [Figure 6.6](#)). maybe 4-panel

6. Helios radial line-up passings

figure?; maybe figures of all into Appendix?

The observed deviations are as expected from these types of solar wind. ...are they? analyze each in

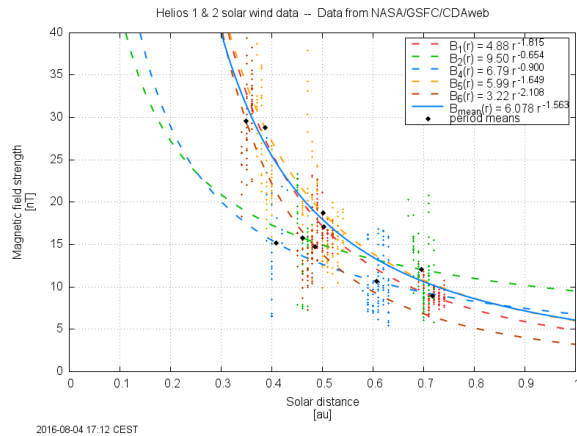


Figure 6.6 Fit curves of the radial magnetic field. The fits are based on the mean values (meanr,meanB; black points) of the line-up periods. build pdf figure... remove date... adjust text size... 4-figure?

detail...

argue from sw type; slow, medium and fast type; check their position relative to the mean curve...

results:

features of calculated line-up periods match.

their derived fit functions scatter within (acceptable?) margin around model's radial mean, backing its applicability.

7 Solar wind impact on the magnetosphere

motivation (see also introduction): solar wind impact nowcast, CME impact forecast

7.1 Solar wind interaction processes with the magnetosphere

As is known for some time the terrestrial magnetic field shows disturbances that are caused by solar wind (see subsection 2.6.1).

there are several underlying physical mechanisms, whose contribution is not yet quantified'?

three ways for solar wind momentum and energy transfer into magnetosphere:

- sw entering sphere
- waves/eddies
- reconnection

-> example events CIR/HSS and CME

7.2 Solar wind–magnetosphere coupling functions

coupling mechanisms and therefrom derived functions
VBzgsm - E-field...

Studies finding best coupling function, Newell, etc.

Newell et al. (2007): universal sw-magnetosphere coupling function (opening flux rate)
Newell et al. (2008): coupling function merging and viscous term
merging and viscous terms (reconnection and turbulence)
merging term: rate magnetic flux is opened at the magnetopause ($d\Phi_{MP}/dt$)
viscous term: reconnection due to Kelvin-Helmholtz instabilities at the boundary ($n^{1/2}v^2$)
equation for the least variance linear prediction of Kp: $Kp = 0.05 + 2.244 \times 10^{-4} d\Phi_{MP}/dt + 2.844 \times 10^{-6} n^{1/2} v^2$
combination of both terms works best ($r = 0.866$)

see also subsection 2.6.4

7.3 Parameter selection

In our analyses we use the planetary geomagnetic disturbance indicator Kp (see Section XX...), because it is designed to measure solar particle radiation by its magnetic effects (cite? Bartels...?). and close relation to aurorae, NOAA scale

choose solar wind parameters based on coupling functions
V, B, Bzgsm, N, T

7.4 Data selection

choose data sets, data resolution and time period

7. Solar wind impact on the magnetosphere

geomagnetic disturbance index Kp: magnetic field maximal variation range within 3 hours; 3-hourly index

need high resolution solar wind data (e.g. 1 min) to be able to determine maximal values/variations within 3 hours

choosing data time range

the Kp time series started in XXXX, when there were no spacecraft to measure in situ solar wind -> time range defined by available solar wind data

OMNI data set -> longest continuous solar wind data set

data processing

choosing data averaging duration and method (min/avg/max)

OMNI 1min data to 3hmin/max

now: 3 hour solar wind extreme value, to back up argument refer to cc table (same data period, different resolution/measure (measure=mean, max or min))

(tested: 3-hour solar wind variation range gives 8 % lower cc)

7.5 General Kp correlations

general frequency distributions

general correlation coefficients + plots

general cc table

7.6 Solar cycle influence

solar cycle dependence

- parameter time plots
- parameter vs SSN matrix-plots
- cc time plots
- cc vs SSN plots

7.7 Isolating the CME influence

the causes of the strongest geomagnetic storms are draping and magnetic clouds of CMEs (Bothmer 1993)

-> example event CME

7.7.1 Solar wind structure list

solar wind structures (SWS) OMNI list of Ian Richardson (Richardson & Cane 2012)

open source 1995–2015 <http://www.srl.caltech.edu/ACE/ASC/DATA/level3/icmetable2.htm>

restricted source 1963–2015 http://cedarweb.vsp.ucar.edu/wiki/index.php/Tools_and_Models:Solar_Wind_Structures Richardson & Cane (2012)

overall CME fraction of solar wind - compute (for used period) from file *sws_swstruc_early63001_4035.txt*
e.g. 2013: 0.220 CMEs, 0.236 CIRs/HSSs and 0.544 slows (low speed streams - LSSs)

7.7.2 CME correlations

same analysis for CMEs

- parameter time plots
- parameter vs SSN matrix-plots
- cc time plots
- cc vs SSN plots

8 Solar wind impact on the terrestrial magnetosphere

Questions:

How strong is the solar wind influence on the terrestrial magnetosphere?

How strong do different structure types influence the terrestrial magnetosphere?

How can the impact strength of the solar wind be forecasted? (VBz->Kp L1-Alerts)

How can the impact strength of CMEs be forecasted (V->Kp correlation for CMEs)?

(How can the impact field strength of CMEs be forecasted (V->B correlation for CMEs)?)

8.1 Quantifying solar wind impact on the terrestrial magnetosphere

linear velocity replacement of ACE realtime data with Kp, Machol2013

3hmin(vBzgsm) performs in rank correlation slightly better than the sophisticated Newell formula

[To quantify this we correlate terrestrial magnetic field measurements with in situ solar wind measurements.]

analyze sw coupling to the magnetosphere (Kp)
coupling functions

choosing data sets:

choosing solar wind parameters
comparison of their correlation coefficients in table...
-> Pearson or Spearman rank cc?? (Appendix?)
-> lag meaning?

What kind of correlation function with these parameters?

comparison of correlation coefficients for different data resolutions and measures in [Table 8.1](#).

Table 8.1 Pearson correlation coefficients of Kp with sample solar wind parameters for different data resolutions and measures for comparison. 3h 1min extrema data results in slightly higher ccs... (use Spearman instead?)

	OMNI 1h 1963-201308 3h mean	OMNI 1h 1963-201308 3h 1h extrema	OMNI 1min 19850101-20150101 3h 10min extrema	OMNI 1min 19850101-20150101 3h 1min extrema
V	0.568	0.579	?	0.598
B				

correlation coefficients in [Table 8.2](#).

resulting figure VBzgsmvsKp; candle flame shape
see [Figure 8.1](#)

correlation coefficient...

8. Solar wind impact on the terrestrial magnetosphere

Table 8.2 Pearson correlation coefficients of Kp with solar wind parameters... (use Spearman instead?)

Parameter	OMNI 1min		
	19850101-20150101		
	3h	1min	max
N	0.199792		
V	0.598351		
T	0.510607		
B	0.595860		
Bzgsm	-0.666050 ^a		
V*B	0.682383		
V*Bzgsm	-0.715101 ^a		
N*T			

^aHere it is min instead of max.

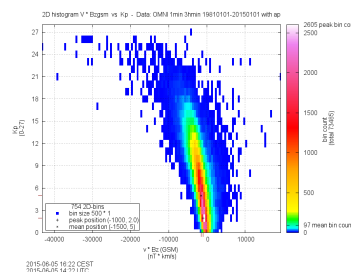


Figure 8.1 Plot fo Kp frequency by V*Bzgsm. make plot flatter...

VBzgsmvsKp dependence plot; V shape
see [Figure 8.2](#)

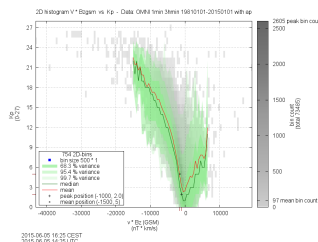


Figure 8.2 Plot like Figure XX but with the Kp dependency.

Results of this section.
What kind of solar wind structures create the individual regions in this distribution? -> next section
What is their individual contribution to the Kp ranges (e.g. high Kp: CMEs 70% and CIRs 30%)?
-> next section

maybe correlation coefficient frequency spectra over time...?

8.2 Solar wind structure type influence on the terrestrial magnetosphere

How strong do different structure types influence the terrestrial magnetosphere?

present single events, avg solar wind and CME
show for both VBzgsmvsKp plot
sws23 VBzgsmvsKp see [Figure 8.3](#)

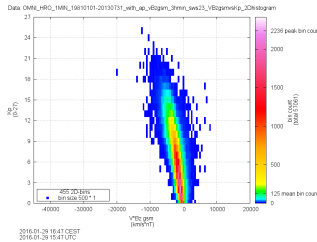


Figure 8.3 same as Figure XX... with the non-CME data flagged by the solar wind structure list. sws23 VBzgsmvsKp

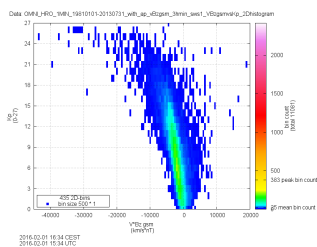


Figure 8.4 same as Figure XX... with the CME data flagged by the solar wind structure list. sws1 VBzgsmvsKp

sws1 VBzgsmvsKp see [Figure 8.4](#)

CME- and non-CME 'comparison' see [Figure 8.5](#)

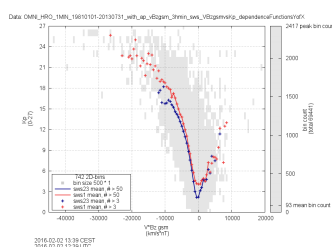


Figure 8.5 Kp dependence on CME- and non-CME structures.

Kp vs VBzgsm - CMEs as fraction of overall solar wind; see [Figure 8.6](#)

8.3 Solar wind structure analyses

ACE solar wind time series (at 1 au) and event list

see OPTIMAP events
?to analyse: ACE event lists

sample CME analyses (MVA, -> Kp)

8.4 CME impact on the magnetosphere

analyze sw coupling to the magnetosphere for being able to estimate CME impact from white light images (see paper draft...)

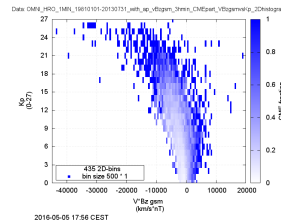


Figure 8.6 CMEs as fraction of overall solar wind. sws1/sws

events from ACE CME list...

add OMNI ap->K_p values and sws flags
 filter to sws1 and sws23 data
 compare CME vs non-CME distributions (VBzgsmvsK_p, VvsK_p, BvsK_p, BzgsmvsK_p..)
 get dependence functions

8.5 Solar wind frequency distributions

How often occur certain conditions?

OMNI hourly data
 v, B, T, n
 see [Figure 8.7](#)



Figure 8.7 Histogram of solar wind velocity.

- overall frequency
- variation over the years (solar cycle)
- seasonal variation
- internal variation (HSS, LSS, CMEs)

8.5.1 Solar wind solar cycle dependence

the density shows no obvious solar cycle dependence (look into it...)
 the parameters V, T and B show a clear solar cycle dependence
 see [Figure 8.8](#) add SSN matrix plot...

8.5.2 Solar wind seasonal dependence

seasonal variation
 SW by month
 quantify variation amplitudes

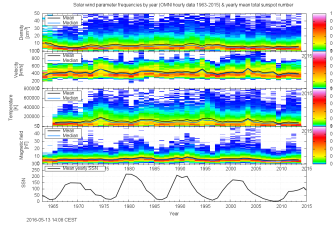


Figure 8.8 Plot of solar wind parameter frequencies and mean total sunspot number by year for the period 1963–2013. Density, velocity, temperature and magnetic field frequencies show more or less a solar cycle dependence, illustrated by the mean total sunspot number. SSN data from WDC-SILSO, Royal Observatory of Belgium, Brussels.

see Figure 8.9

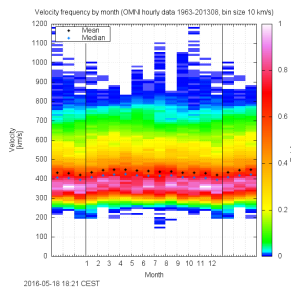


Figure 8.9 Diagram of the velocity frequency by month for the period 1963/01–2013/08. Mean and median values are shown as well.

derived exponent values from simple trigonometric fit on monthly values:
 $c_N = -2.234$
 maybe figure?

...following maybe into section 'radial dependence of median value?
 expected influence from perihelion/aphelion (see Appendix...) distance vs observations
 we expect for the proton density (scaling law $N(r) = 7.6 \text{ cm}^{-3} \cdot r^{-2}$):
 $N(0.983 \text{ au}) = 7.9 \text{ cm}^{-3}$
 $N(1 \text{ au}) = 7.6 \text{ cm}^{-3}$
 $N(1.017 \text{ au}) = 7.3 \text{ cm}^{-3}$
 we expect for the magnetic field strength (scaling law $\propto r^{-1.6}$):
 $B(0.983 \text{ au}) = 6.3 \text{ nT}$
 $B(1 \text{ au}) = 6.1 \text{ nT}$
 $B(1.017 \text{ au}) = 5.9 \text{ nT}$

see Figure 8.10

8.6 Kp frequency distribution

Plot of the Kp frequency distribution (see Figure 8.11)

8.6.1 Kp solar cycle dependence

- solar cycle variations
- variations between solar cycles

the yearly Kp frequency shows variations; the yearly mean Kp shifts about 2 units.
 plot of the yearly Kp frequency (see Figure 8.12) add Kp–SSN matrix plot...

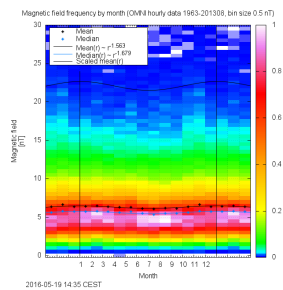


Figure 8.10 Diagram of magnetic field frequency by month for the period 1963/01–2013/08. Mean and median values are shown as well as the expected course from the solar distance variation (obtained from Helios data).

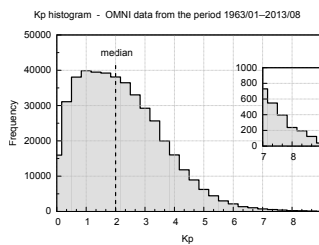


Figure 8.11 Kp frequency distribution for the period 1963/01–2013/08. The median Kp value is 2 and a Kp of 90 occurred only 39 times. OMNI data.

analyze Kp frequency by month for different SWSs
 analyze Kp frequency by year for different SWSs
 put into later part of analysis...

8.6.2 Kp seasonal dependence

for high Kp values (> 4 ?) there are yearly frequency maxima at the equinoxes and minima at the solstices. this variation amounts to more than 1 Kp (see Figure 8.13)

possible causes (see Rangarajan & Iyemori (1997) p. 1282 and mention Bartels1963 too):

- Earth's rotation axis tilt ($\pm 23.44^\circ$) (obliquity to orbit/inclination of equator)
- solar rotation axis tilt ($\pm 7.25^\circ$) (cite 'NASA Earth fact sheet')
- varying distance from Sun 0.983–1.0167 au ($\pm 3.3\%$)
- changing solar cycle polarity gives two superimposed maxima... -> No. see even/odd plots

read Bothmer1998 Ch 3...

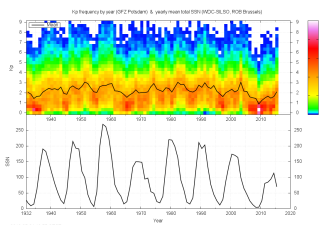


Figure 8.12 Kp frequency by year, yearly mean Kp and yearly mean total SSN for the years 1932–2015. The pattern of Kp shows an imprint of the solar cycle. Kp data from GFZ German Research Centre for Geosciences, Potsdam, Germany and SSN data from WDC-SILSO, Royal Observatory of Belgium, Brussels.

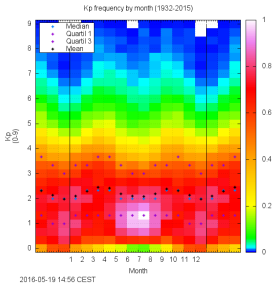


Figure 8.13 Diagram of Kp frequency by month for the period 1932–2015. Median and quartil values are shown as well. remove mean...

8.7 Summary/Results

sw-nowcast: vBzgsm-Kp relation (average and worst case)
CME-forecast: v-Kp relation (average and worst case)

seasonal correction: $\Delta Kp(\text{month})$
 $Kp_{\text{impact}} = Kp_{\text{CME}} \pm \Delta Kp(\text{month})$

sw-timeseries ACE OPTIMAP “Zeitreihe”-events

8.8 Forecast

8.8.1 Internal solar wind correlations

B-V correlation
ACE MAGSWE 64 s data -> yearly overlay plot

8.8.2 Kp forecast from CME velocity

V-Kp correlation
similar to [Elliott et al. \(2013\)](#); different data resolution and averaging method (3-hour maximum of 1 min data)

8.9 Applications

rssfeeds, rtsw plots
CME Kp impact
part of DDC

9 Solar wind origin and evolution

talk about origin and evolution...

what is the aim?

- empirical analytical sw distribution model with radial dependence
- sw extrapolation to near-Sun region with an empirical sw model

Motivation?

- solar wind acceleration
- coronal heating problem
- SPP mission

new analyses of the Helios solar wind data

input (Helios data):

magnetic field strength; proton velocity, number density and temperature

output (results):

empirical distribution model for 0.29–0.98 au

empirical distribution extrapolation model to near-Sun region

L-> refined models with the combination of OMNI data

theory/literature:

existing model: ([Sittler & Guhathakurta 1999](#))

L-> compare with their radial density function eq. (18a)

existing solar wind and CME measurements, steady state mass flow (eq. (5)), velocity model $v(r)$ ([Sheeley et al. 1997](#))

Helios results, radial gradients see Schwenn1990 p. 155

Schwenn1983 intro -> sw-averaging comment (beer and wine)

)

[Balogh et al. \(1999\)](#) (origin and formation of CIRs in inner heliosphere with Helios data)

see Hellinger2013 p.1353

see Balogh1999 from p. 162

and what differentiates our model from the others...

model constraints:

see Marsch1999...

9.1 Solar wind parameters

motivation/reason for necessity?/why?

which parameters? (major solar wind parameters)

- The characteristic behavior of a plasma is determined by its density, temperature and magnetic field strength. cite?
- the velocity is the defining parameter of the solar wind

definition of 'the four solar wind parameters':

magnetic field strength, aka magnetic field, B , usually measured in nT, in the order of 0–35 nT at 1 au

9. Solar wind origin and evolution

proton bulk velocity, aka velocity, v , usually measured in km/s, in the order of 200–900 km/s at 1 au
proton number density, aka density, n , usually measured in cm $^{-3}$, in the order of 1–60 at 1 au
proton temperature, aka temperature, T , usually measured in K, in the order of 10 000–1 000 000 K at 1 au
sentence about ordering of the parameters...

hourly OMNI data
measurement precision:
 B : 0.01 nT
 v : 1 km/s
 n : 0.1 cm $^{-3}$
 T : 1 K ? (smallest found: 7 K)

error discussion:
OMNI hourly data mean:
 B : bin size 0.5 nT, median 5.6, mean 6.30056(18)
 v : bin size 10 km/s, median 414, mean 437.6700(18)
 n : bin size 1 cm $^{-3}$, median 5.3, mean 6.831410(18)
 T : bin size 10 000 K, median 80 751, mean 112 219.0(19) (with 1000 K as precision)

empirical data; Helios; hourly
why hourly and not higher resolution data?
measurement precision:
 B : 0.01 nT
 v : 0.1 km/s
 n : 0.1 cm $^{-3}$
 T : 100–1000 K (3 digits)
 r : 0.01 au

error discussion:
Helios hourly data mean:
 B : min 337, precision: 0.000545; 18.3x better
 v : min 497, precision: 0.00449; 22.2x
 n : min 497, precision: 0.00449; 22.2x
 T : min 497, precision: 4.49–44.49 22.2x
=> so we use 1/10 the measurement precision for the mean.

median precision same as data precision

9.2 Empirical solar wind model

Helios data ranges:
- time range [1974-12-10–1980-03-04]
- solar distance range 0.29–0.98 au
- 0°–360° longitude
- latitude range -7.25°–7.25°
data constrictions:
- hourly data
- data gaps => uneven coverage => solar cycle minimum dominates
- limited parameter ranges

model boundaries (spherical coordinates):
- mean solar wind of the Helios time range
- solar distance range 0.29–0.98 au
- rotational symmetry
- confined to ecliptic
model constrictions:

- radial dependency function
- frequency distribution function

all assumptions outside these boundaries are extrapolations with large uncertainties...

influence from latitude variation in data negligible? (see Ulysses figure in introduction). Helios probes within ecliptic => variation span equal to solar tilt: -7.25° to 7.25° ; solar tilt/obliquity to ecliptic: $i_\odot = 7.25^\circ$ (Sun fact sheet: <http://nssdc.gsfc.nasa.gov/planetary/factsheet/sunfact.html>)

big part of Helios data is from latitudes $> \pm 5^\circ$, see Figure XX (data count over latitude) and see Figure XX (Helios orbit polar plane in data section...)

As we see at the end of this chapter in Section XX, the latitude influence is negligible and so we assume it to be constant for our models.

see also Richardson et al. (1995)

see also Schwenn (1990) p. 127

approach:

- determine fit function type for radial dependency of Helios data
- determine fit function type for frequency distribution of OMNI data
- fit exponential radial double lognormal function to binned Helios data
- evaluation of function behavior in direction of Sun up to 0.04 au
- single lognormal fit with constant width is extrapolation model
- model evaluation
- some model variants with OMNI median values

9.2.1 Solar distance dependency—theory

heliospheric distance r

averages: median(r), mean(r)

solar wind parameter distributions and their radial dependence from theory/literature:

B-field radial profile: $B \propto r^{-5/2}$

Kivelson/Parker references

shear effect from solar rotation; talk 2014-07-21

velocity radial profile: $V \propto r^{0.5}$

model based on LeBlanc1998 electron density with flux conservation: Zic2015(Temmer)

Parker...

density radial profile: $N \propto r^{-2}$

simple view: for a spherical constant velocity mass outflow a one over distance squared law is expected because of the mass flux conservation per solid angle for different distances. measurements up to the outer heliosphere confirm the $1/r^2$ dependency (1–38 au by Voyager 2, (Belcher et al. 1993) newer paper?)

electron density model corona–1 au LeBlanc1998

radial electron density from Helios $6.14r^{-2.10}$ compared to radio bursts see Bougeret1983

existing electron density model see Leblanc1998

in an ideal neutral plasma the electron and proton number density have the same values (neutral plasma) (reference?)

ca. 10 % more electrons than protons (due to alphas) cite?

radial electron density models suggest a proportionality to r^{-2} for $r > 10 R_\odot$ (leblanc1998 with its Figure 6)

temperature radial profile: $T \propto r^{-1.5}$

at larger distances heating outbalances the adiabatic temperature part (adiabatic cooling vs. pickup proton and stream–interaction heating; 1–68 au by Voyager 2; Richardson & Smith (2003))

solar wind ram pressure $p_{\text{ram}} = \rho V^2$

conserved quantities:

- momentum conservation... VBbookp112
- flux conservation...

With consideration of continuity the mass flux per solid angle has to be constant: $\dot{m} = \text{const}$
conserved quantities:

- mass flux: $\dot{m} = \rho v A$ (with mass density ρ , velocity v and [cross-sectional area A] or solid angle?...)
- particle fluxes (proton flux, electron flux, etc.)
- proton flux: $j_p = n_p v_p A$ (with proton density n_p and proton velocity v_p)

(with proton mass density $\rho = n_p m_p$ (with proton number density n_p and proton mass m_p)).

the individual radial dependencies for a spherical radial outflow are:

$$A(r) \propto r^2 \rightarrow A/r^2 = \text{const}$$

and assuming an exponential dependency,

$$n_p(r) = n_0 r^{c_n},$$

$$v(r) = v_0 r^{c_v}$$

$$j_p = \text{const} \quad (9.1)$$

$$n_p v_p A = \text{const} \quad (9.2)$$

$$n_0 r^{c_n} v_0 r^{c_v} r^2 = \text{const} \quad (9.3)$$

$$r^{c_n} r^{c_v} r^2 = \text{const} \quad (9.4)$$

$$\Rightarrow c_n + c_v + 2 = 0 \quad (9.5)$$

$$c_n + c_v = -2 \quad (9.6)$$

an increasing velocity should result in a steeper density...

validity of mass flux continuity: within the heliosphere mass to energy conversion and vice versa is negligible, but there can be flux from and to higher latitudes as the Helios data is localized to a small latitude range in the ecliptic plane.

estimate the error from that... (if error is too big => drop continuity condition)

larger errors should be located near CMEs and CIRs (nonradial flows from interactions)

there is a proton flux difference between slow and fast solar wind streams (see book Schwenn1990 p. 146)

estimate the possible size of error:

mean:

$$c_n = -2.010$$

$$c_v = 0.049$$

$$c_n + c_v = -1.961$$

difference to -2 is 0.039

9.2.2 Solar distance dependency—Helios data

we want to obtain the solar distance dependence of the mean and the median of the Helios data

we use hourly Helios data...

the hourly Helios data has a native radial resolution of 0.01 au, so for calculating the median the data is binned into 0.01 au bins

we expect an exponential behavior from all four parameters (see radial dependence theory section with literature references)

=> therefore we use an exponential regression fit function $f(r) = a r^b$.
fit weighting by counts per bin

the resulting fit curves are displayed in [Figure 9.1](#). Larger individual Graphs can be found in the appendix (Figures XX).

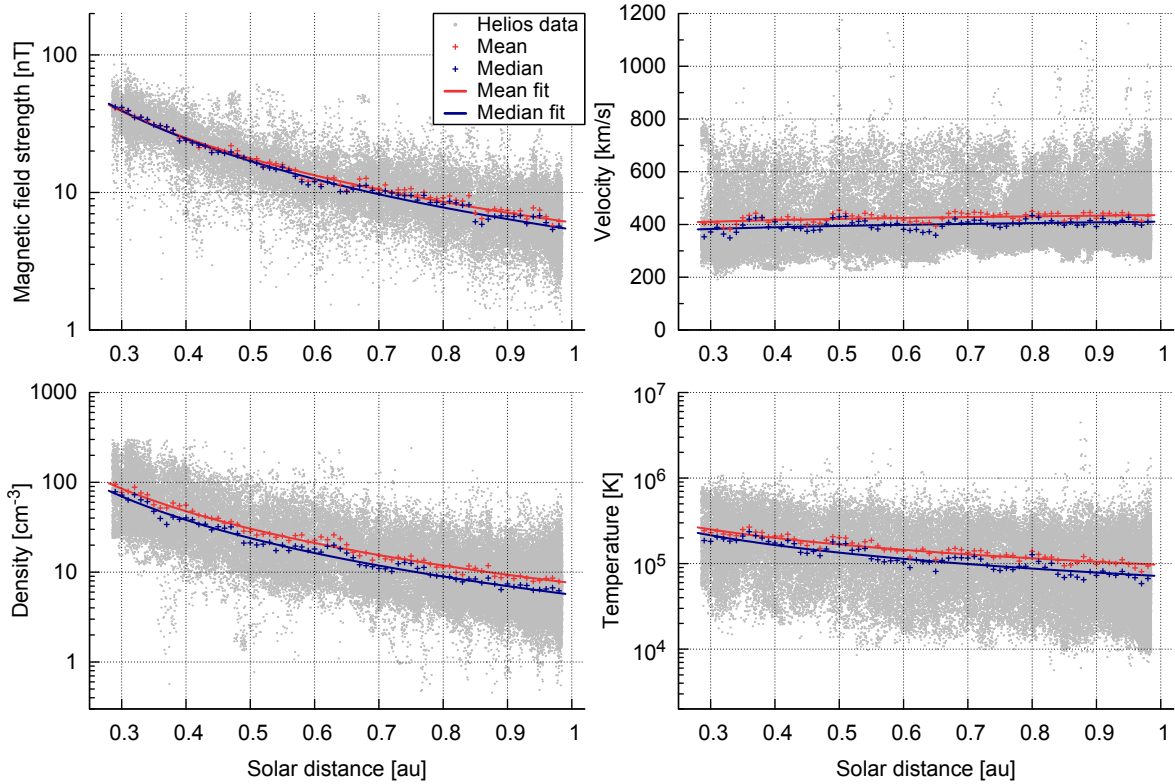


Figure 9.1 Plots of the four solar wind parameters over solar distance. The mean and median per 0.1 au data bin and their fit curves (weighted with data count) are plotted as well.

flux figure...

With r in astronomical units one gets the fit coefficient values of all four parameters as seen in Table 9.1.

Table 9.1 These are the fit coefficients for the median and mean solar distance dependence functions of the four plasma parameters from the combined Helios data set. The errors in brackets are the estimated standard deviation of each fit parameter. remove units?

Parameter	Median		Mean		r_{equal}
	a	b	a	b	
Magnetic field	5.377(92) nT	-1.655(17)	6.05(10) nT	-1.546(18)	0.344 au
Velocity	410.7(28) km/s	0.058(13)	435.6(24) km/s	0.049(10)	692 au
Density	5.61(27) cm ⁻³	-2.093(46)	7.57(30) cm ⁻³	-2.010(38)	0.027 au
Temperature	$7.14(23)\times 10^4$ K	-0.913(39)	$9.67(21)\times 10^4$ K	-0.792(28)	0.081 au
Flux	fit coeffients...				

skewing of distributions...
 its change...
 for the magnetic field strength the mean and median cross each other at 0.344 au.

9.2.3 Latitude dependency—theory

refer to Ulysses figure...
 Ulysses swoops polar plots...
 see Schwenn1990's Fig. 3.14

9.2.4 Latitude dependency—Helios data

latitude; see Figure 9.2

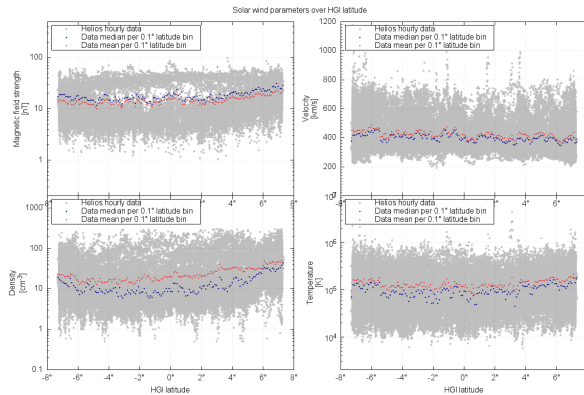


Figure 9.2 The four solar wind parameter's HGI latitude dependency. Their mean values per 0.1° bin are plotted as well. make figure same dimensions as projected figure in analysis part...

with the exponential dependencies to 1 au projected solar wind parameters; there are only small changes with latitude in the range -7.25° – 7.25°

have a look on distribution widths...

dependence from latitude in interval -7.25° – 7.25° in Helios data negligible?, see Figure 9.3. estimate

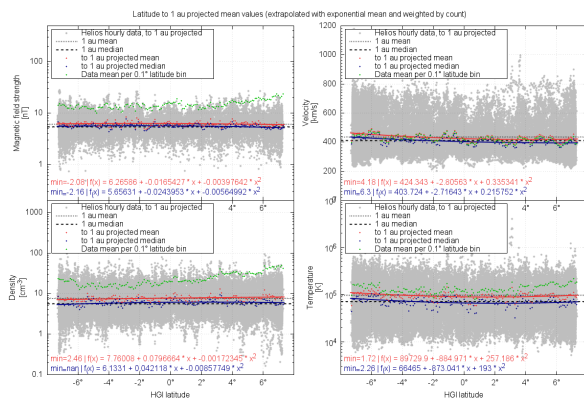


Figure 9.3 Plot of the to 1 au projected solar wind parameters over latitude. And their mean values, including weighted fit. add projected median...

error ranges...

plot Ulysses data into plot...

9.2.5 Shape of the frequency distributions

getting shape of the general distributions.

fitting the shape of the parameter's frequency distribution

Obviously the possible values for all four parameters are positive. This hints to the supposition that they are lognormally distributed, as many positive natural quantities conform to a lognormal distribution. This distribution is described by the lognormal function (For more on lognormal distributions see appendix section B.2).

Therefore we use the lognormal function as a fit function in the process of the least squares regression fitting.

To evaluate how well the lognormal function represents the solar wind distributions, the abundance of OMNI data (>50 years at 1 au) is more suited than the Helios data (few weeks summed at fixed solar distance), because it enables the averaging over long-time variations like the solar cycle. As basis for the fit in situ solar wind data from the OMNI data set is used (see Section XX... data section). More precisely, it is hourly data of the whole time range 1963/01–2013/08.

Helios histogram bin size for mean of frequency distribution (at specific solar distance)

B : bin size 0.5 nT, min 337, mean precision: 0.000545

v : bin size 1 cm $^{-3}$, min 497, mean precision: 0.00449

n : bin size 10 km/s, min 497, mean precision: 0.00449

T : bin size 10 000 K, min 497, mean precision: 4.49–44.49

Single lognormal fit

The lognormal fit function

$$W(x) = \frac{1}{\sigma\sqrt{2\pi}} e^{-\frac{(\ln x - \mu)^2}{2\sigma^2}} \quad (9.7)$$

has two variables, the location (μ) and the shape parameter (σ) (see also Appendix XX). The distribution's mean and median positions are easier to interpret and can directly be calculated from μ and σ (see also Appendix XX):

$$\text{median} = e^\mu$$

$$\text{mean} = e^{\left(\mu + \frac{\sigma^2}{2}\right)}$$

Their values, obtained from the fitting of the four solar wind frequency distributions, are listed in Table 9.2.

Table 9.2 These are the resulting fit coefficients μ and σ from the fitting of the lognormal function (9.7) to the shape of the frequency distributions. The median and mean values and the standard deviation of the fit are shown as well. The values in brackets are the estimated standard deviation of each parameter.

Parameter	μ	σ	Median ^a	Mean ^a	stdfit [10 $^{-3}$]
Magnetic field	1.7361(28)	0.4150(24)	5.675(16)	6.186(19)	1.3
Velocity	6.0146(49)	0.2182(40)	409.4(20)	419.2(21)	2.9
Density	1.6660(47)	0.6448(39)	5.291(25)	6.514(35)	1.7
Temperature	11.2917(19)	0.9086(16)	$8.015(15) \times 10^4$	$1.2111(29) \times 10^5$	0.16

^aValues in their respective units nT, km/s, cm $^{-3}$ and K.

describe figures; see Figure 9.4

From visual inspection, the resulting curves match well with the shape of the magnetic field strength, density and temperature distributions (Figure 9.4). But for the velocity the fit function seems insufficient in describing its more complex shape.

From the normed stdfit values (Table 9.2) the velocity...

discuss high-value tail figures...

To reach better fit results for the velocity the fit function has to be changed. We do not want to abandon the well-founded application of lognormal functions. But it is reasonable to assume that the distributions are composed of multiple branches (why?; slow/fast solar wind; literature; introduction). Therefore a compositional approach promises better fit results, which is why in the following we combine two lognormal functions.

Double lognormal fit

why only two? -> to keep it simple; every additional function adds further fit variables
compositional (two functions) lognormal regression fit

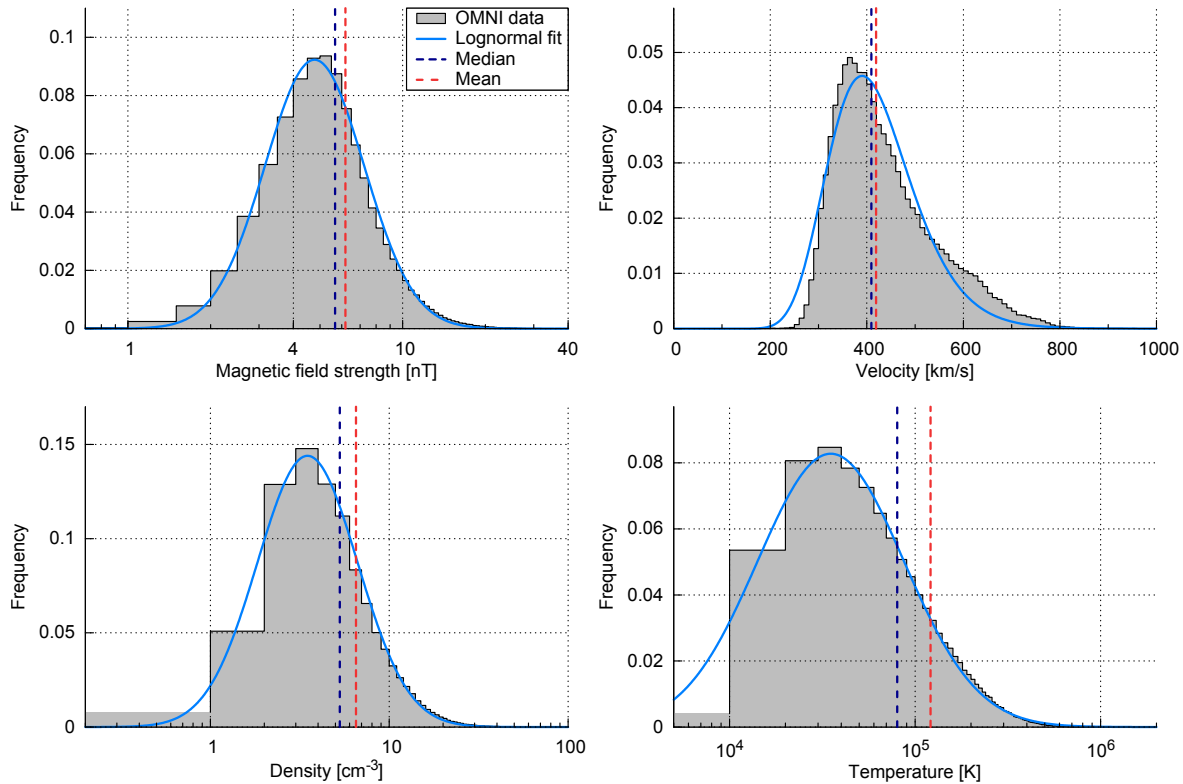


Figure 9.4 The frequency distributions of the four solar wind parameters and their lognormal fits. The histograms have bins of 0.5 nT, 10 km/s, 1 cm^{-3} and 10 000 K and are based on the hourly OMNI data set. The fit's median and mean values are indicated as well.

For the compositional regression fitting we use a function $W_{\text{II}}(x)$ which is composed of two lognormal distributions $W_1(x)$ and $W_2(x)$. The balancing parameter c ensures that the resulting function remains normalized.

$$W_{\text{II}}(x) = c \cdot W_1(x) + (1 - c) \cdot W_2(x) \quad (9.8)$$

$$= \frac{c}{\sigma_1 \sqrt{2\pi}} e^{-\frac{(\ln x - \mu_1)^2}{2\sigma_1^2}} + \frac{(1 - c)}{\sigma_2 \sqrt{2\pi}} e^{-\frac{(\ln x - \mu_2)^2}{2\sigma_2^2}} \quad (9.9)$$

The fitting of $W_{\text{II}}(x)$ to the frequency distributions gives the values of the five fit parameters ($c, \sigma_1, \mu_1, \sigma_2, \mu_2$), which are listed in [Table 9.3](#).

The median of the composed distribution can be derived via solving

$$\int W_{\text{II}}(x) dx = 0 \quad (9.10)$$

and the mean via solving

$$\int x W_{\text{II}}(x) dx = 0. \quad (9.11)$$

Their values are listed in [Table 9.3](#).

The fitted functions show [a good match] for the parameters, [even for the velocity] (see Figure XX). how good fits the function to the shape? discuss figures...

goodness of fit; discuss high value zoom figures

To be able to compare the goodness of the single with the compositional lognormal fits we make use of their corresponding sum of squared residuals (SSR). More precisely the 'reduced SSR' where the SSR is divided by the number of degrees of freedom to account for the data set size and the fit function complexity (for more on SSRs see Appendix [section B.3](#)). As anticipated, the reduced SSR

Table 9.3 These are the resulting fit coefficients from the double lognormal function (9.9) for the four examined solar wind parameters. The derived median and mean values are listed as well. Precision? Fit error in brackets.

Parameter	fkt	c	μ	σ	Median ^a	Mean ^a	stdfit [10^{-4}]
Magnetic field	f1	0.8656(79)	1.7450(13)	0.4631(23)	5.6570(X)	6.769(X)	3.1
	f2	-	1.6981(26)	0.2061(50)			
Velocity	f1	0.502(59)	5.911(27)	0.138(14)	413.4(X)	439.1(X)	6.6
	f2	-	6.1997(52)	0.2117(40)			
Density	f1	0.751(70)	1.817(40)	0.6970(88)	5.337(X)	8.784(X)	8.7
	f2	-	1.372(27)	0.459(34)			
Temperature	f1	0.669(11)	10.9368(98)	0.7691(54)	$8.081(X) \times 10^4$	$1.667(X) \times 10^5$	1.2
	f2	-	11.968(12)	0.6007(42)			

^aValues in their respective units nT, km/s, cm⁻³ and K.

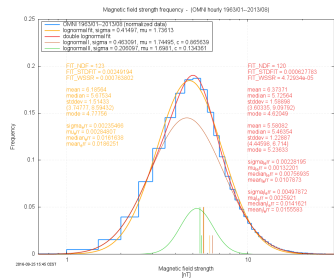


Figure 9.5 Plot of the double lognormal fit on the magnetic field strength frequency distribution. 3:2

values of the composed fit are considerably smaller. The evaluation of the ratio of the reduced SSRs of the respective single and double fits shows that indeed the double fits are 3.7–19.1 times more accurate (see Table 9.4).

Table 9.4 The reduced SSR for the single and the double lognormal fit and their ratio. use stdfit for comparison...

Parameter	single SSR _{red}	double SSR _{red}	ratio s/d
Magnetic field	7.64×10^{-4}	4.73×10^{-5}	16.15
Velocity	8.41×10^{-6}	4.41×10^{-7}	19.07
Density	3.23×10^{-4}	8.67×10^{-5}	3.73
Temperature	8.34×10^{-13}	8.97×10^{-14}	9.30

Especially the velocity and the magnetic field strength benefit from the more complex fit function. When is the single fit sufficient? -> maybe evaluate from absolute goodness of fit...

9.2.6 Helios solar wind model

Helios data, radial binned and frequency binned

Fit on the solar distance and frequency using the balancing parameter c from the compositional shape fit before (see equation (9.9)).

=> fit function with solar distance dependency

to be able to make the model's radial dependency exponential, we fit not μ and σ but the median ($\tilde{x}, x^{\text{med}}, x_{\text{med}}, \xi?$) and mean (\bar{x}) of both lognormal functions to the data. As these parameters can be derived from each other directly, equation (9.9) with the replacing relations

$$\tilde{x} = e^\mu \quad \Rightarrow \quad \mu = \ln(\tilde{x}) \quad (9.12)$$

$$\bar{x} = e^{(\mu + \frac{\sigma^2}{2})} \quad \Rightarrow \quad \sigma = \sqrt{2 \ln \left(\frac{\bar{x}}{\tilde{x}} \right)} \quad (9.13)$$

results in

$$W_{\text{II}}(x, \tilde{x}_1, \bar{x}_1, \tilde{x}_2, \bar{x}_2) = \frac{c}{2\sqrt{\pi \ln\left(\frac{\tilde{x}_1}{\bar{x}_1}\right)} x} \exp\left(-\frac{\ln^2\left(\frac{x}{\tilde{x}_1}\right)}{4 \ln\left(\frac{\tilde{x}_1}{\bar{x}_1}\right)}\right) + \frac{(1-c)}{2\sqrt{\pi \ln\left(\frac{\tilde{x}_2}{\bar{x}_2}\right)} x} \exp\left(-\frac{\ln^2\left(\frac{x}{\tilde{x}_2}\right)}{4 \ln\left(\frac{\tilde{x}_2}{\bar{x}_2}\right)}\right) \quad (9.14)$$

introducing the radial exponential dependency of the mean and median

$$\tilde{x}_1(r) = \tilde{a}_1 r^{\tilde{b}_1} \quad (9.15)$$

$$\bar{x}_1(r) = \bar{a}_1 r^{\bar{b}_1} \quad (9.16)$$

$$\tilde{x}_2(r) = \tilde{a}_2 r^{\tilde{b}_2} \quad (9.17)$$

$$\bar{x}_2(r) = \bar{a}_2 r^{\bar{b}_2} \quad (9.18)$$

we get the ultimate monster equation:

$$W_{\text{II}}(x, \tilde{a}_1, \tilde{b}_1, \bar{a}_1, \bar{b}_1, \tilde{a}_2, \tilde{b}_2, \bar{a}_2, \bar{b}_2) = \quad (9.19)$$

$$\frac{c}{2\sqrt{\pi \ln\left(\frac{\tilde{a}_1 r^{\tilde{b}_1}}{\bar{a}_1 r^{\bar{b}_1}}\right)} x} \exp\left(-\frac{\ln^2\left(\frac{x}{\tilde{a}_1 r^{\tilde{b}_1}}\right)}{4 \ln\left(\frac{\tilde{a}_1 r^{\tilde{b}_1}}{\bar{a}_1 r^{\bar{b}_1}}\right)}\right) + \frac{(1-c)}{2\sqrt{\pi \ln\left(\frac{\tilde{a}_2 r^{\tilde{b}_2}}{\bar{a}_2 r^{\bar{b}_2}}\right)} x} \exp\left(-\frac{\ln^2\left(\frac{x}{\tilde{a}_2 r^{\tilde{b}_2}}\right)}{4 \ln\left(\frac{\tilde{a}_2 r^{\tilde{b}_2}}{\bar{a}_2 r^{\bar{b}_2}}\right)}\right) \quad (9.20)$$

the model represents the data well, see Figure 9.6

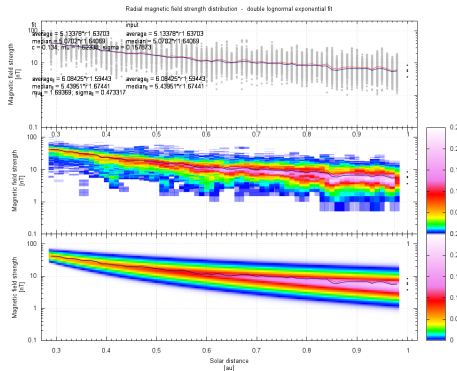


Figure 9.6 Plot of the magnetic field strength over solar distance. The top panel shows the hourly data from both Helios spacecraft, their median and their mean values. The second panel shows the same data binned into 0.1 au and 0.5 nT bins. The bins are normalized for distance, i.e. the bin values represent the frequency of getting the bin magnitude at that distance. The bottom panel shows the exponential double lognormal function (XX), which is obtained from fitting to the data. insert keys... adjust color scale... keep log x scale?

The resulting fit coefficients for all four solar wind parameters are presented in Table 9.5.

The model's amplitude differences to the data are becoming larger with smaller solar distance (check it.), see Figure 9.7

comparison with simple radial mean and median

The distribution width varies with heliospheric distance (back up with figure!).

We see that the density and temperature shapes stay almost constant...

varying shape with distance is indicator for internal physical processes (mixing/turbulence...)

Table 9.5 These are the resulting fit coefficients from the compositional function (XX). precision... Fit error in brackets? 2-line table if fit errors do not reduce it enough...

Plasma parameter	c	$W_1(x, r)$				$W_2(x, r)$			
		median		mean		median		mean	
		a	b	a	b	a	b	a	
Magnetic field strength	0.866	5.43951	-1.67441	6.08425	-1.59443	5.0702	-1.64069	5.13378	-1.64069
Velocity	0.502	370.994	0.114544	373.556	0.107352	480.016	-0.0151313	494.135	-0.0151313
Density	0.751	6.75345	-2.17915	8.13399	-2.19658	3.09089	-2.12598	3.42042	-2.12598
Temperature	0.669	41 262.8	-1.18491	58 852.7	-1.32940	141 238	-0.570392	168 399	-0.570392

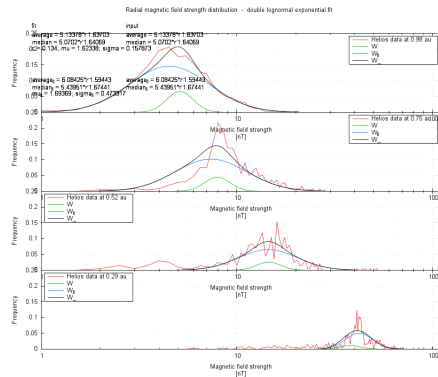


Figure 9.7 Plot of the magnetic field strength's frequency distribution at different solar distances (0.29, 0.52, 0.75 and 0.98 au). The Helios data, the composed fit model and both its components are plotted. 0.23 au steps, lw 2, stepfunction

Model quality

self-consistency?; model assumptions valid?

limitations: The model is valid within the heliospheric distance range of 0.29–0.98 au in the ecliptic plane (with maximal errors of...). average hourly values.

validity and estimation of error size outside of valid model range...
spatial ranges:

- radial range of model validity (extrapolation boundaries)
- latitude range...

Model extrapolation to near-Sun region (and Mars orbit?)

expanding the range of the model to the Sun leads to a singularity, see **Figure 9.8** that is caused by

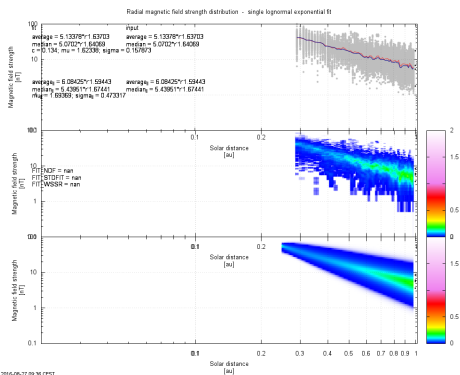


Figure 9.8 expanding the range of the model to the Sun leads to a singularity... expand range to >2 au...

the convergence and eventually crossing of median(r) and mean(r)

for the magnetic field strength the mean and median cross each other at 0.246 au. below that point it cannot be lognormally distributed anymore, because for lognormal functions always applies mean > median (see Section XX)

=> what kind of distribution has the B-field near the Sun?

9.3 Extrapolation model

for the extrapolation it is better to use a single lognormal function, because:

- extrapolation error so big that additional accuracy would not matter
- [easier to compute the mean(r) and median(r); otherwise numerical determination]
- model easier to modify for different time ranges
- ...

new requirement: possibility to extrapolate the model to the near-Sun region
to avoid the crossing of median(r) and mean(r), their exponents b have to be identical (constant width)
 $\text{median}(r) = X_{\text{med},0} r^b$
 $\text{mean}(r) = \text{mean}_0 r^b$

fit function here...

So the new fit function has only the three fit parameters median_0 , mean_0 and b .

The resulting fit coefficients for all solar wind parameters are presented in [Table 9.6](#).

Table 9.6 The resulting fit coefficients from the single lognormal fit of function (XX). constant width... Standard fit error in brackets.

Parameter	\tilde{x}_0^{a}	\bar{x}_0^{a}	b
Magnetic field	5.358(25)	5.705(28)	-1.662(11)
Velocity	399.1(17)	411.7(18)	0.0711(71)
Density	5.424(33)	6.845(47)	-2.114(20)
Temperature	$6.357(64) \times 10^4$	$1.072(14) \times 10^5$	-1.100(20)

^aValues in their respective units nT, km/s, cm⁻³ and K.

frequency distribution, see [Figure 9.9](#)

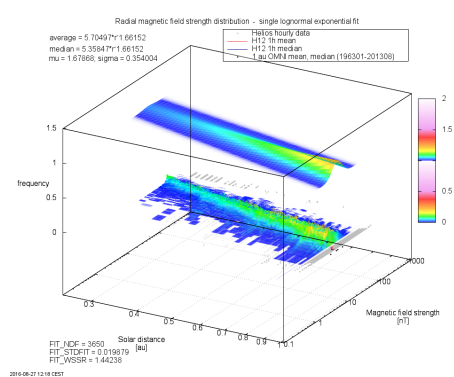


Figure 9.9 remove 3d plot, make 2d Plot of the magnetic field strength's frequency distribution at different solar distances (0.29, 0.52, 0.75 and 0.98 au). The Helios data and the single lognormal fit model with constant width are plotted. 0.23 au steps, stepfunction

single fit model with constant width, see [Figure 9.10](#)

W error

B stdfit error: 0.020

B error at (1 au,Bmean): 0.011

B error at (1 au,Bmedian): 0.011

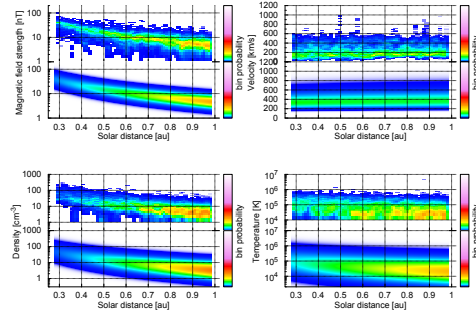


Figure 9.10 The solar wind parameter's frequency distribution over solar distance. The Helios data and the single lognormal fit model with constant width are plotted.

max data – model deviation: 0.011

see Figure 9.11

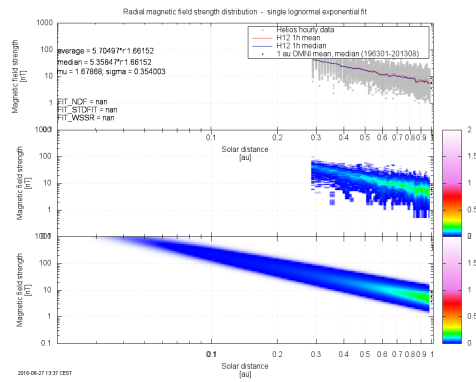


Figure 9.11 Plot of the magnetic field strength over solar distance (similar to Figure XX). The top panel shows the same data binned into 0.1 au and 0.5 nT bins. The bins are normalized for distance, i.e. the bin values represent the frequency of getting the bin magnitude at that distance. The bottom panel shows the exponential single lognormal function (XX) with constant width, which is obtained from fitting to the data. insert keys... adjust color scale... keep log x scale? remove top panel...

quartile fit extrapolation...

expected values at 0.04 au...

9.3.1 Model validity

validity and estimation of error size outside of valid model range...

The extrapolation distance is only about one third of the model range, but as the parameters follow exponential change, one has to look at the logarithmic distance which is indeed one and a half times the model range.

argument with gravitational deceleration; near-Sun extrapolation should be biased, because in the near-Sun region gravitation becomes significant (see Figure 9.12)

polar plot with highlighted model range and 1-3 extrapolation extensions... (for both models)

9.3.2 Model comparison via SSR

model comparison via the reduced SSR for the fit parameters from Tables 9.6 and 9.5, see Table 9.7

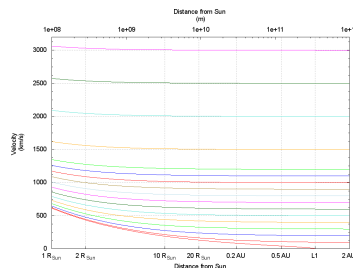


Figure 9.12 velocity over solar distance; gravitational deceleration. place instead figure of grav. force over solar distance...

Table 9.7 The reduced SSR for the Helios model and the extrapolation model fits and their ratio. precision...

Plasma parameter	Helios model SSR_{red}	Extrapolation model SSR_{red}	ratio Helios/extrapolation
Magnetic field strength	1.18	1.44	1.22
Velocity	2.66×10^{-3}	3.47×10^{-3}	1.30
Density	2.54×10^{-1}	2.67×10^{-1}	1.05
Temperature	2.14×10^{-9}	2.35×10^{-9}	1.10

9.3.3 Adjusted extrapolation models

extrapolation models for different time spans:
extrapolation with OMNI data and solar cycle/seasonal variations

9.3.4 Comparison with existing extrapolation models

comparison with s.o. elses values...
...with Vourlidas estimates at $10 R_\odot$
...with Wang2000 slow blobs

9.4 Radial evolution of solar wind structures

Radial evolution of solar wind structures from Helios data

Helios event lists HSSs, SLOWs, CIRs, CMEs...; event lists for all Helios data
see Liu2004 for Helios ICME list and radial dependencies of B, n, T and v...

200 km/s slow solar wind at $10 R_\odot$ is in agreement with blob measurements from Wang2000

very slow sw (VSSW) gets accelerated; see Sanchez-Diaz2016:

structure extrapolations

radial diameter of MCs increase between 0.3 au and 4.3 au proportional to the distance as $r^{0.8}$
(Bothmer & Schwenn 1998)

MC central axial magnetic field strength radial density dependence $B = 18.1 r^{-1.64}$ Leitner et al. (2007)

MC average diameter $D = 0.23 r^{1.14}$ Leitner et al. (2007)

sw structure marked plot

9.5 Summary/Results

where does the solar wind get accelerated? (at 3–4 R_s for moving density enhancements (slow solar wind), see Sheeley1997)

results beneficial for Solar Probe Plus (SPP) mission which is to investigate coronal heating and the origin of the solar wind

SPP will have its closest perihelion at 9.86 solar radii (0.0459 au), see [Fox et al. \(2015\)](#)

10 Discussion/conclusions/results

discussion
conclusions
results

Prediction:
Link from near-Sun solar wind measurements to Kp impact
Link from near-Sun structure (CMEs, CIRs) measurements to Kp impact

11 Summary and outlook

Outlook

DSCOVR data (advantages over ACE? gain?)
anticipated Solar Probe Plus data (near-Sun data)

other possible space weather missions: sub-L1 (earlier in situ CME magnitude warning) and L5 (early CME velocity and arrival warning)

I built an empirical solar wind model for the ecliptical inner heliosphere which accounts for variations in time (season and solar cycle) and space (solar distance).

Using the SSN prediction the model allows the forecast and extrapolation of the solar wind, which will occur during the SPP mission's first near-Sun perihelia in mid-2018.

A Physics

A.1 Electromagnetism

Electromagnetism is one of the four fundamental forces at the common level of energy. In all situations examined in this thesis (sw plasma, magnetosphere) it is by far the strongest force and the others can be neglected.

The Lorentz force: $\mathbf{F} = q(\mathbf{E} + \mathbf{v} \times \mathbf{B})$

The Maxwell equations in differential notation:

$$\operatorname{div} \mathbf{B} = 0 \quad (\text{A.1})$$

$$\operatorname{div} \mathbf{D} = \rho \quad (\text{A.2})$$

$$\operatorname{rot} \mathbf{H} = \mathbf{j} + \dot{\mathbf{D}} \quad (\text{A.3})$$

$$\operatorname{rot} \mathbf{E} = -\dot{\mathbf{B}} \quad (\text{A.4})$$

With the magnetic flux density \mathbf{B} (aka magnetic field), the electric displacement field \mathbf{D} , the charge density ρ , the magnetic field \mathbf{H} , the electric field \mathbf{E} and the current density \mathbf{j} .

A.2 Solar wind pressures

The magnetic energy density w_{mag} is also the magnetic pressure p_{mag}

$$w_{\text{mag}} = p_{\text{mag}} \quad (\text{A.5})$$

$$= \frac{B^2}{2\mu_0}. \quad (\text{A.6})$$

dynamic pressure $p_{\text{dyn}} = \rho v^2$
 thermal pressure $p_{\text{therm}} = nk_B T$
 magnetic pressure $p_{\text{mag}} = B^2/(2\mu_0)$ (see above...)
 ram pressure??

A.3 Plasma beta

In MHD the magnetic energy density behaves like an additional pressure that adds to the gas pressure of a plasma (Wikipedia; find alternative source...).

The ratio of the thermal pressure $p = nk_B T$ to the magnetic pressure $p_{\text{mag}} = \frac{B^2}{2\mu_0}$ is called plasma beta

$$\beta = \frac{p}{p_{\text{mag}}} \quad (\text{A.7})$$

$$= \frac{2\mu_0 n k_B T}{B^2} \quad (\text{A.8})$$

with the number density n .

$\beta \ll 1$: “cold” plasma; magnetic field contains plasma (magnetic clouds)

$\beta \geq 1$: “warm” plasma; plasma keeps magnetic field

plasma beta see ([Kivelson & Russell 1995](#), p. 50)

typical *beta*-values for solar wind are in the range X–Y.

A.4 Alfvén waves

named after Hannes Alfvén...

There exists an incompressible wave mode which is a result of bending magnetic field lines called shear Alfvén wave.

In an ideal incompressible MHD plasma (viscosity $\mu = 0$ and electrical conductivity $\sigma = \infty$) the kinetic and magnetic energy density are of equal value:

$$w_{\text{kin}} = w_{\text{mag}} \quad (\text{A.9})$$

$$\frac{\rho v^2}{2} = \frac{B^2}{2\mu_0}$$

with the permeability constant

$$\mu_0 = 4\pi \cdot 10^{-7} \text{ N A}^{-2}$$

and the total mass density ρ of the charged plasma particles.

So waves propagate with the so-called Alfvén velocity

$$v_A = \frac{|B|}{\sqrt{\mu_0 \rho}}. \quad (\text{A.10})$$

Their phase velocity is

$$v_{\text{ph}} = v_A \cos(\theta) \quad (\text{A.11})$$

with θ the angle between wave propagation direction (k) and magnetic field line (B). \Rightarrow Alfvén waves travel along magnetic field lines. Alfvén waves are characterized by periodic disturbances in the magnetic field perpendicular to its direction, in the electric field, in the plasma velocity and in the current density. They do not affect the plasma density, plasma pressure and magnetic field magnitude.

Additionally, there exist two types of compressional waves within MHD plasmas, the fast-mode wave and the slow-mode wave. The phase speeds of the three MHD waves meet $v_{\text{fast}} \geq v_A \geq v_{\text{slow}}$.

Alfvén waves are dominant in regions that are open to the heliosphere.

Alfvén waves see (Kivelson & Russell 1995, pp. 51ff.)

Within average solar wind at 1 au their typical frequency is 1–4 per hour (cite?) ($v_A = 53 \text{ km/s}$ for $B = 5.6 \text{ nT}$ and $\rho = 5.3 \text{ cm}^{-3}$).

critical surfaces, solar wind acceleration...

A.5 Solar surface differential rotation

the solar rotation was first discovered from sunspots in 18XX?

Bartels (1934) set the synodic solar rotation period to 27 days for the definition of his solar rotation number. The Bartels' Rotation Number counts the solar rotations starting with 8 February 1832. Carrington solar rotation period of 27.2753 days (Where Carrington Rotation Number is based upon, starting with November 9, 1853; Wikipedia...)

Solar surface rotation period at 16° latitude:

sidereal: 25.38 d (of 609.12 h Sun Fact Sheet...), synodic: 27.2753 d (derived)

rotation axis tilt (see next section)

The Sun's inner thermal convective circulation results in a differential rotation caused by transport of angular momentum away from the rotation axis.

The Sun's sidereal differential angular velocity best-fitting function with values as stated in (Sun Fact Sheet...)¹ is

$$\omega_{\odot} = A + B \sin^2(b) + C \sin^4(b) \quad (\text{A.12})$$

¹NASA's Sun Fact Sheet (<http://nssdc.gsfc.nasa.gov/planetary/factsheet/sunfact.html>, accessed 2016-08-19).

with the latitude b , the equatorial angular velocity $A = 14.37^\circ/\text{d}$, the coefficients $B = -2.33^\circ/\text{d}$ and $C = -1.56^\circ/\text{d}$ (see Figure A.1).

see Figure A.1

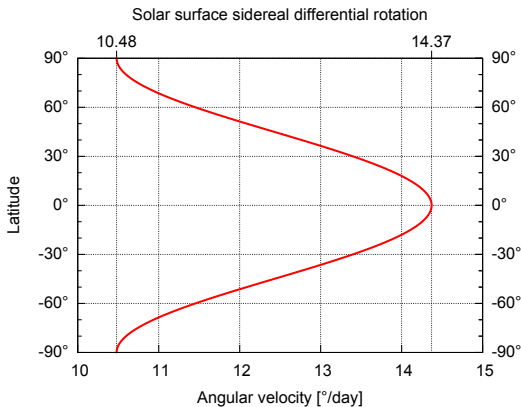


Figure A.1 Diagram of the sidereal solar surface differential rotation. It shows the angular velocity for different latitudes.

Thus, the solar equatorial rotation period (sidereal) is

$$\begin{aligned} T_{\odot}^{\text{eq}} &= 360^\circ/A \\ &= 25.05 \text{ d} \end{aligned} \quad (\text{A.13})$$

and the synodic period is

$$\begin{aligned} T_{\odot}^{\text{eq,syn}} &= 1/(1/T_{\odot}^{\text{eq}} - 1/T_{\text{Earth}}) \\ &= 26.90 \text{ d} \end{aligned} \quad (\text{A.14})$$

with the Earth's orbital rotation period $T_{\text{Earth}} = 365.25 \text{ d}$ (1/100 Julian century).

Solar surface rotation period at equator
sidereal: 25.05 d (Sun Fact Sheet...), synodic: 26.90 d (derived)

Solar surface rotation period at poles:
sidereal: 34.35 d (diff. rot. formula), synodic: 37.92 d (derived)
are listed in Table A.1.

Table A.1 Solar surface rotation periods for equator, $\pm 16^\circ$ latitude and poles (sidereal and synodic).

	Equator [d]	$\pm 16^\circ$ latitude [d]	Poles [d]
Sidereal	25.05	25.38	34.35
Synodic	26.90	27.2753 ^a	37.92

^aCarrington solar rotation period

The meridional circulation is the proposed equatorial updrift and polar downdrift - a result of Reynolds stress and convective transport (cite?).

A.6 Earth orbit geometry

orbit defines ecliptic

Earth orbit parameters (cite?):
semimajor axis: $a = 1.000001018 \text{ au}$
eccentricity: $e = 0.0167086 \text{ au}$
distance at perihelion: (formula cite?, accuracy?)

$$\begin{aligned} r_p &= a(1 - e) \\ &= 0.98329 \text{ au} \end{aligned} \tag{A.15}$$

distance at aphelion:

$$\begin{aligned} r_p &= a(1 + e) \\ &= 1.0167 \text{ au} \end{aligned} \tag{A.16}$$

for calculation of heliospheric distance see HORIZONS Web-Interface at <http://ssd.jpl.nasa.gov/horizons.cgi>
perihelion/aphelion times...

A.6.1 Solar distance

A.6.2 Solar rotation axis tilt

The inclination of the solar equator to the ecliptic (tilt/obliquity) is $i_{\odot} = 7.25^\circ$ ([U.S. Nautical Almanac Office 2015](#)).

Viewed from Earth the projected solar rotation axis tilt angle varies as the Earth is moving on its orbit.

At the time XX the angle is zero.

The projected tilt angle to Earth over the year is

Hapgood (1992):

$$\omega = 73.67 + 0.013958 * (\text{today} - 1850.0) \tag{A.17}$$

solar tilt over the year, see [Figure A.2](#)

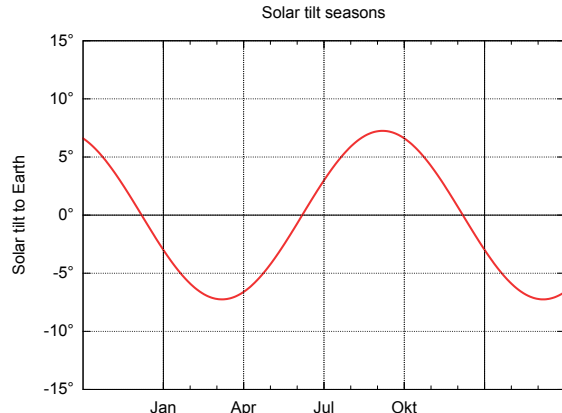


Figure A.2 Projected solar tilt angle over the year as viewed from Earth. remove sides...

A.6.3 Earth tilt

A.7 Coordinate systems

Coordinate systems used in this thesis:

GSE - Geocentric Solar Ecliptic

GSM - Geocentric Solar Magnetospheric

HGI - Heliographic Inertial

refer to [Hapgood \(1992\)](#) for GSE and GSM

figures for GSE and GSM

A.7.1 Geocentric Solar Ecliptic

The Geocentric Solar Ecliptic (GSE) coordinates are
GSE - Geocentric Solar Ecliptic
X = Earth-Sun Line
Z = Ecliptic North Pole
GSE coordinates are used in ACE solar wind data, etc.

A.7.2 Geocentric Solar Magnetospheric

GSM - Geocentric Solar Magnetospheric
X = Earth-Sun Line
Z = Projection of dipole axis on GSE YZ plane

GSM is defined with a time dependent dipole axis.
the dipole axis orientation changes over time; at 1995 the northern pole was at $l = 288.59^\circ$ and
 $b = 79.30^\circ$; more recent year (2015)?... cite?

A.7.3 Heliographic Inertial

HGI - Heliographic Inertial coordinates

B Math

B.1 Correlations

auto correlation

cross correlation

Pearson linear correlation

Spearman rank correlation

Correlation in Linear Regression: <http://www.stat.yale.edu/Courses/1997-98/101/correl.htm>

B.2 Lognormal distribution

This is a small summary about the lognormal probability distribution (Bronstein et al. 2000, p. 780). The lognormal distribution is the distribution of a random variable X if the logarithm of X conforms to a normal distribution. Its shape is highly asymmetric, however in a semi-log plot the Gaussian bell curve is recognizable (see the second panel of Figure B.1). Its probability density function is

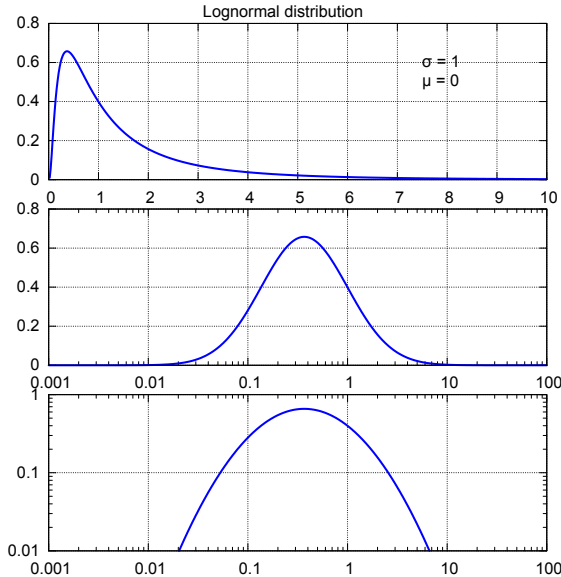


Figure B.1 The lognormal probability density function ($\sigma = 1, \mu = 0$) plotted in a linear, semi-log and log-log way.

$$f(x) = \frac{1}{\sigma\sqrt{2\pi}x} e^{-\frac{(\ln x - \mu)^2}{2\sigma^2}} \quad (\text{B.1})$$

with the location (μ) and the shape parameter (σ). Changes in μ affect both the horizontal and vertical scaling of the function, whereas σ has an influence on its shape (see Figure B.2).

Because it is a probability distribution, its area is normalized

$$\int_0^\infty f(x)dx = 1. \quad (\text{B.2})$$

For a lognormally distributed random variable the geometric moments mean, standard deviation

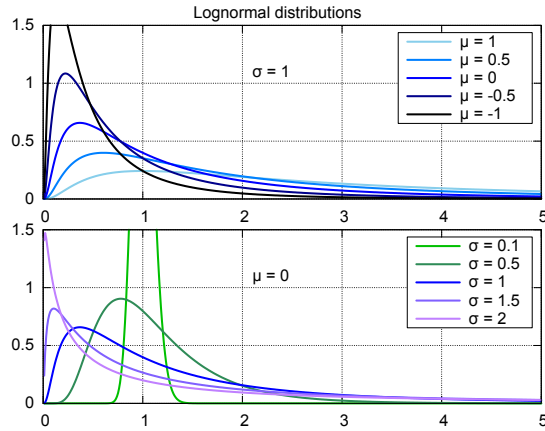


Figure B.2 Five lognormal distributions plotted with fixed σ (top) and fixed μ (bottom).

and variance are:

$$\begin{aligned}\mu_g &= e^\mu, \\ \sigma_g &= e^\sigma, \\ var_g &= e^{\sigma^2} \quad (!).\end{aligned}$$

Its arithmetic moments are:

$$\begin{aligned}\mu_a &= e^{\mu + \frac{\sigma^2}{2}}, \\ \sigma_a &= e^{\mu + \frac{\sigma^2}{2}} \left(e^{\sigma^2} - 1 \right), \\ var_a &= \sigma_a^2.\end{aligned}$$

Other useful characteristics are the median and the mode

$$\begin{aligned}x_{\text{median}} &= e^\mu, \\ x_{\text{mode}} &= e^{\mu - \sigma^2}.\end{aligned}$$

Note that for the lognormal distribution its median is equal to its geometric mean.

Applications of lognormal distributions...

Most natural quantities which can only be positive are lognormally distributed. e.g. animal body sizes?, animal life expectancies, financial stock prices...; income distributions.

B.3 Goodness of fit

SSR – sum of squared residuals

$$SSR = \sum_i (y_i - f_i)^2 \tag{B.3}$$

data values y_i , fit function values f_i

SSR_{red} – reduced SSR, divided by number of degrees of freedom ν

$$SSR_{\text{red}} = \frac{SSR}{\nu} \tag{B.4}$$

TSS – total sum of squares (in relation to the data mean)

$$TSS = \sum_i (y_i - \bar{y})^2 \quad (\text{B.5})$$

with data mean \bar{y}

χ^2 – chi-square

χ_{red}^2 – reduced chi-square, divided by number of degrees of freedom ν

R^2 – coefficient of determination

$0 \leq R^2 \leq 1$, “values can be less than zero”!. if $R^2 = 1 \rightarrow$ ideal fit; if $R^2 = 0 \rightarrow$ bad fit

$$R^2 = 1 - \frac{SSR}{TSS} \quad (\text{B.6})$$

“In case of a single regressor, fitted by least squares, R^2 is the square of the Pearson product-moment correlation coefficient relating the regressor and the response variable.” cite from wikipedia

Kolmogorov-Smirnov K-S-Test

B.4 other

minimum variance analysis (MVA)

determining magnetic cloud configuration ([Bothmer & Schwenn 1998](#))

hodogramm?

least-squares fit approximates mean linear regression

robust statistics

Non-parametric inferential statistical methods are mathematical procedures for statistical hypothesis testing which make no assumptions about the probability distributions of the variables being assessed. The most frequently used tests include - median - percentiles (quartiles) - Spearman’s rank correlation coefficient

histogram

generalized mean http://en.wikipedia.org/wiki/Generalized_mean

normal distribution

C Glossary

C.1 Astronomical constants

Astronomical unit: $1 \text{ au} = 149\,597\,870\,700 \text{ m}$ ([U.S. Nautical Almanac Office 2015](#))

Solar mass: $M_{\odot} = 1.9884(2) \times 10^{30} \text{ kg}$ ([U.S. Nautical Almanac Office 2015](#))

Nominal solar radius (photosphere): $R_{\odot} = 695\,700 \text{ km}$ ([Mamajek et al. 2015](#))

Sun escape velocity: $v_{\text{esc}} = 617.6 \text{ km/s}$ (Sun Fact Sheet...)

Solar rotation axis tilt: $i_{\odot} = 7.25^\circ$ ([U.S. Nautical Almanac Office 2015](#))

Solar surface rotation period at equator, sidereal: 25.05 d (Sun Fact Sheet...)

Nominal solar effective temperature (photosphere): $T_{\text{eff}\odot} = 5772 \text{ K}$ ([Mamajek et al. 2015](#))

C.2 Symbols

s/c - spacecraft

B - magnetic field strength

n - number density

...

C.3 Abbreviations

Projects:

AFFECTS Advanced Forecast For Ensuring Communications Through Space

HELCATS Heliographic Cataloging, Analysis and Techniques Service

FP7 Framework Programme 7

CGAUSS Coronagraphic German And US SolarProbePlus Survey

OPTIMAP OPerational Tool for Ionospheric Mapping And Prediction

Spacecraft:

SPP – Solar Probe Plus

WISPR – Wide-field Imager for Solar Probe

ACE – Advanced Composition Explorer

MAG – Magnetometer

SWEPAM – Solar Wind Electron Proton Alpha Monitor

RTSW – Real Time Solar Wind

SDO – Solar Dynamics Observatory

SOHO – Solar and Heliospheric Observatory

STEREO – Solar TErrestrial RElations Observatory

Organizations:

NASA – National Aeronautics and Space Administration

SPDF – Space Physics Data Facility

NOAA – National Oceanic and Atmospheric Administration

SWPC – Space Weather Prediction Center

UGOE – University of Göttingen

IAG – Institute for Astrophysics Göttingen

GFZ – GeoForschungsZentrum

WDC-SILSO – World Data Center-Sunspot Index and Long-term Solar Observations

Sun:

DB – disparition brusques (disappearing filaments?; quiescent filaments?)

C. Glossary

SSN – sunspot number

Solar wind:

IMF – interplanetary magnetic field

CME – coronal mass ejection

ICME – interplanetary coronal mass ejection

MC – magnetic cloud

HSS – high speed stream

CIR – corotating interaction region

SIR – stream interaction region

SB – sector boundary

BDE – bidirectional electrons

HCS – heliospheric current sheet

HPS – heliospheric plasma sheet

Earth:

Kp – planetare Kennziffer

Dst – Disturbance storm time

Coordinate systems:

GSE – geocentric solar ecliptic

GSM – geocentric solar magnetospheric

Theories and techniques:

MVA – minimum variance analysis

MHD – magnetohydrodynamic

GCS – Graduated Cylindrical Shell

CAT – CME Analysis Tool

References

- Bahcall, J. N., Pinsonneault, M. H. & Wasserburg, G. J. 1995, *Solar models with helium and heavy-element diffusion*, Reviews of Modern Physics, 67, 781, <http://adsabs.harvard.edu/abs/1995RvMP...67..781B>.
- Balogh, A. & Jokipii, J. R. 2009, *The Heliospheric Magnetic Field and Its Extension to the Inner Heliosheath*, Space Sci. Rev., 143, 85, <http://adsabs.harvard.edu/abs/2009SSRv..143...85B>.
- Balogh, A., Bothmer, V., Crooker, N. U. et al. 1999, *The Solar Origin of Corotating Interaction Regions and Their Formation in the Inner Heliosphere*, Space Sci. Rev., 89, 141, <http://adsabs.harvard.edu/abs/1999SSRv...89..141B>.
- Banaszkiewicz, M., Axford, W. I. & McKenzie, J. F. 1998, *An analytic solar magnetic field model*, Astron. Astrophys., 337, 940, <http://adsabs.harvard.edu/abs/1998A%26A...337..940B>.
- Bartels, J. 1934, *Twenty-seven day recurrences in terrestrial-magnetic and solar activity, 1923-1933*, Terrestrial Magnetism and Atmospheric Electricity (Journal of Geophysical Research), 39, 201, <http://adsabs.harvard.edu/abs/1934TeMAE..39..201B>.
- . 1962, *Zur Vorgeschichte der Weltraumforschung*, Naturwissenschaften, 49, 313, <http://adsabs.harvard.edu/abs/1962NW.....49..313B>.
- Bartels, J. & Veldkamp, J. 1949, *International Data on Magnetic Disturbances, First Quarter, 1949*, J. Geophys. Res., 54, 295, <http://adsabs.harvard.edu/abs/1949JGR....54..295B>.
- Belcher, J. W., Lazarus, A. J., McNutt, Jr., R. L. & Gordon, Jr., G. S. 1993, *Large-scale density structures in the outer heliosphere*, Advances in Space Research, 13, 41, <http://adsabs.harvard.edu/abs/1993AdSpR..13...41B>.
- Billings, D. E. 1959, *Distribution of Matter with Temperature in the Emission Corona.*, Astrophys. J., 130, 961, <http://adsabs.harvard.edu/abs/1959ApJ...130..961B>.
- Bothmer, V. 1993, *Die Struktur magnetischer Wolken im Sonnenwind: Zusammenhang mit eruptiven Protuberanzen und Einfluß auf die Magnetosphäre der Erde*, PhD thesis, Georg-August-Universität Göttingen, <http://hdl.handle.net/11858/00-001M-0000-0014-F2C4-2>.
- Bothmer, V. & Daglis, I. A. 2007, *Space Weather – Physics and Effects* (Praxis Publishing), <http://adsabs.harvard.edu/abs/2007swpe.book.....B>, doi:10.1007/978-3-540-34578-7.
- Bothmer, V. & Schwenn, R. 1998, *The structure and origin of magnetic clouds in the solar wind*, Annales Geophysicae, 16, 1, <http://adsabs.harvard.edu/abs/1998AnGeo..16....1B>.
- Bronstein, I. N., Semendjajew, K. A., Musiol, G. & Mühlig, H. 2000, *Taschenbuch der Mathematik* (Verlag Harri Deutsch), <https://books.google.de/books?id=zCKyuQAACAAJ>.
- Christensen-Dalsgaard, J., Gough, D. O. & Thompson, M. J. 1991, *The depth of the solar convection zone*, Astrophys. J., 378, 413, <http://adsabs.harvard.edu/abs/1991ApJ...378..413C>.
- Christensen-Dalsgaard, J., Dappen, W., Ajukov, S. V. et al. 1996, *The Current State of Solar Modeling*, Science, 272, 1286, <http://adsabs.harvard.edu/abs/1996Sci...272.1286C>.
- Cranmer, S. R. & van Ballegooijen, A. A. 2005, *On the Generation, Propagation, and Reflection of Alfvén Waves from the Solar Photosphere to the Distant Heliosphere*, Astrophys. J., Suppl. Ser., 156, 265, <http://adsabs.harvard.edu/abs/2005ApJS..156..265C>.
- Danziger, I. J. 1970, *The Cosmic Abundance of Helium*, Ann. Rev. Astron. Astrophys., 8, 161, <http://adsabs.harvard.edu/abs/1970ARA%26A...8..161D>.

References

- Elliott, H. A., Jahn, J.-M. & McComas, D. J. 2013, *The K_p index and solar wind speed relationship: Insights for improving space weather forecasts*, Space Weather, 11, 339, <http://adsabs.harvard.edu/abs/2013SpWea..11..339E>.
- Fox, N. J., Velli, M. C., Bale, S. D. et al. 2015, *The Solar Probe Plus Mission: Humanity's First Visit to Our Star*, Space Sci. Rev., doi:10.1007/s11214-015-0211-6, <http://adsabs.harvard.edu/abs/2015SSRv..tmp..105F>.
- Gurnett, D. A., Kurth, W. S., Burlaga, L. F. & Ness, N. F. 2013, *In Situ Observations of Interstellar Plasma with Voyager 1*, Science, 341, 1489, <http://adsabs.harvard.edu/abs/2013Sci...341.1489G>.
- Hapgood, M. A. 1992, *Space physics coordinate transformations - A user guide*, Planet. Space Sci., 40, 711, <http://adsabs.harvard.edu/abs/1992P%26SS...40..711H>.
- Hathaway, D. H. 2015, *The Solar Cycle*, Living Reviews in Solar Physics, 12, 4, <http://adsabs.harvard.edu/abs/2015LRSP...12....4H>.
- King, J. H. & Papitashvili, N. E. 2005, *Solar wind spatial scales in and comparisons of hourly Wind and ACE plasma and magnetic field data*, Journal of Geophysical Research (Space Physics), 110, 2104, <http://adsabs.harvard.edu/abs/2005JGRA..110.2104K>.
- Kivelson, M. G. & Russell, C. T. 1995, *Introduction to Space Physics* (Cambridge University Press), <http://adsabs.harvard.edu/abs/1995isp..book.....K>.
- Leitner, M., Farrugia, C. J., Möstl, C. et al. 2007, *Consequences of the force-free model of magnetic clouds for their heliospheric evolution*, Journal of Geophysical Research (Space Physics), 112, 6113, <http://adsabs.harvard.edu/abs/2007JGRA..112.6113L>.
- Lem, S. & Kandel, M. 1984, *His Master's Voice* (Houghton Mifflin Harcourt), <http://books.google.de/books?id=nzgLf4zKph0C>.
- Mamajek, E. E., Prsa, A., Torres, G. et al. 2015, *IAU 2015 Resolution B3 on Recommended Nominal Conversion Constants for Selected Solar and Planetary Properties*, ArXiv e-prints, arXiv:1510.07674, <http://adsabs.harvard.edu/abs/2015arXiv151007674M>.
- Maunder, E. W. 1904, *Note on the distribution of sun-spots in heliographic latitude, 1874-1902*, Mon. Not. R. Astron. Soc., 64, 747, <http://adsabs.harvard.edu/abs/1904MNRAS..64..747M>.
- McComas, D. J., Ebert, R. W., Elliott, H. A. et al. 2008, *Weaker solar wind from the polar coronal holes and the whole Sun*, Geophys. Res. Lett., 35, L18103, <http://adsabs.harvard.edu/abs/2008GeoRL..3518103M>.
- Miesch, M. S. 2005, *Large-Scale Dynamics of the Convection Zone and Tachocline*, Living Reviews in Solar Physics, 2, 1, <http://adsabs.harvard.edu/abs/2005LRSP....2....1M>.
- Newell, P. T., Sotirelis, T., Liou, K., Meng, C.-I. & Rich, F. J. 2007, *A nearly universal solar wind-magnetosphere coupling function inferred from 10 magnetospheric state variables*, Journal of Geophysical Research (Space Physics), 112, A01206, <http://adsabs.harvard.edu/abs/2007JGRA..112.1206N>.
- Newell, P. T., Sotirelis, T., Liou, K. & Rich, F. J. 2008, *Pairs of solar wind-magnetosphere coupling functions: Combining a merging term with a viscous term works best*, Journal of Geophysical Research (Space Physics), 113, A04218, <http://adsabs.harvard.edu/abs/2008JGRA..113.4218N>.
- Opher, M., Drake, J. F., Swisdak, M. et al. 2011, *Is the Magnetic Field in the Heliosheath Laminar or a Turbulent Sea of Bubbles?*, Astrophys. J., 734, 71, <http://adsabs.harvard.edu/abs/2011ApJ...734...71O>.
- Owens, M. J. & Forsyth, R. J. 2013, *The Heliospheric Magnetic Field*, Living Reviews in Solar Physics, 10, 5, <http://adsabs.harvard.edu/abs/2013LRSP...10....5O>.
- Parker, E. N. 1958, *Dynamics of the Interplanetary Gas and Magnetic Fields.*, Astrophys. J., 128, 664, <http://adsabs.harvard.edu/abs/1958ApJ...128..664P>.

- Pizzo, V. J. 1991, *The evolution of corotating stream fronts near the ecliptic plane in the inner solar system. II - Three-dimensional tilted-dipole fronts*, J. Geophys. Res., 96, 5405, <http://adsabs.harvard.edu/abs/1991JGR....96.5405P>.
- Planck Collaboration, Ade, P. A. R., Aghanim, N. et al. 2016, *Planck 2015 results. XIII. Cosmological parameters*, Astron. Astrophys., 594, A13, <http://adsabs.harvard.edu/abs/2016A&26A...594A..13P>.
- Rangarajan, G. K. & Iyemori, T. 1997, *Time variations of geomagnetic activity indices K_p and A_p : an update*, Annales Geophysicae, 15, 1271, <http://adsabs.harvard.edu/abs/1997AnGeo..15.1271R>.
- Richardson, I. G. & Cane, H. V. 2012, *Near-earth solar wind flows and related geomagnetic activity during more than four solar cycles (1963–2011)*, Journal of Space Weather and Space Climate, 2, A2, <http://adsabs.harvard.edu/abs/2012JSWSC...2A..02R>.
- Richardson, I. G., Cliver, E. W. & Cane, H. V. 2000, *Sources of geomagnetic activity over the solar cycle: Relative importance of coronal mass ejections, high-speed streams, and slow solar wind*, J. Geophys. Res., 105, 18203, <http://adsabs.harvard.edu/abs/2000JGR...10518203R>.
- Richardson, J. D., Paularena, K. I., Lazarus, A. J. & Belcher, J. W. 1995, *Radial evolution of the solar wind from IMP 8 to Voyager 2*, Geophys. Res. Lett., 22, 325, <http://adsabs.harvard.edu/abs/1995GeoRL..22..325R>.
- Richardson, J. D. & Smith, C. W. 2003, *The radial temperature profile of the solar wind*, Geophys. Res. Lett., 30, 1206, <http://adsabs.harvard.edu/abs/2003GeoRL..30.1206R>.
- Schatten, K. H., Wilcox, J. M. & Ness, N. F. 1969, *A model of interplanetary and coronal magnetic fields*, Solar Phys., 6, 442, <http://adsabs.harvard.edu/abs/1969SoPh....6..442S>.
- Schwenn, R. 1983, *The average solar wind in the inner heliosphere: Structures and slow variations*, in NASA Conference Publication, Vol. 228, NASA Conference Publication, <http://adsabs.harvard.edu/abs/1983NASCP.2280.489S>.
- Schwenn, R. 1990, *Large-Scale Structure of the Interplanetary Medium*, ed. R. Schwenn & E. Marsch, Physics of the Inner Heliosphere I, 99, <http://adsabs.harvard.edu/abs/1990pihl.book...99S>.
- Sheeley, N. R., Wang, Y.-M., Hawley, S. H. et al. 1997, *Measurements of Flow Speeds in the Corona Between 2 and 30 R_\odot* , Astrophys. J., 484, 472, <http://adsabs.harvard.edu/abs/1997ApJ...484..472S>.
- Sittler, Jr., E. C. & Guhathakurta, M. 1999, *Semiempirical Two-dimensional MagnetoHydrodynamic Model of the Solar Corona and Interplanetary Medium*, Astrophys. J., 523, 812, <http://adsabs.harvard.edu/abs/1999ApJ...523..812S>.
- Thompson, M. J., Christensen-Dalsgaard, J., Miesch, M. S. & Toomre, J. 2003, *The Internal Rotation of the Sun*, Ann. Rev. Astron. Astrophys., 41, 599, <http://adsabs.harvard.edu/abs/2003ARA%26A..41..599T>.
- U.S. Naval Observatory. 2015, *Astronomical Almanac for the Year 2016 and Its Companion, the Astronomical Almanac Online* (United States Department of Defense), https://books.google.de/books?id=Mc_VuQN_gVsC.
- Zhao, J., Bogart, R. S., Kosovichev, A. G., Duvall, Jr., T. L. & Hartlep, T. 2013, *Detection of Equatorward Meridional Flow and Evidence of Double-cell Meridional Circulation inside the Sun*, Astrophys. J., Lett., 774, L29, <http://adsabs.harvard.edu/abs/2013ApJ...774L..29Z>.

Acknowledgments

I thank

my supervisor Volker Bothmer
the committee (Ansgar Reiners, second?)
the proofreaders

The author like to thank the proofreaders for very helpful comments and suggestions.
the 'Büro' for cozily accomodating me all the long hours

for creating and making scientific data available:

- SWS list (see Acknowledgements in Elliott2013; directly Ian Richardson)
- OMNI data (see paper)
- ACE data
- Helios data (see paper)
- Kp data
- SSN data

I acknowledge the financial support from the projects

AFFECTS: Solar wind correlation with magnetosphere

CGAUSS: Solar wind model and extrapolation

HELCATS: Minimum variance analyses of magnetic clouds

OPTIMAP: Solar wind ACE time series

This work was done within the scope of the CGAUSS project, funded by the German Aerospace Center (grant number...).

The authors thank the Helios and OMNI teams for creating and making availabe the solar wind in situ data. The Helios and the OMNI data sets were supplied by the Space Physics Data Facility at NASA's Goddard Space Flight Center.

We thank the 'referees' for /important comments and suggestions. /careful review of this paper.

facilities/persons which made available the Helios and OMNI data

"Ian Richardson and Hilary Cane for making their Interplanetary Coronal Mass Ejection list readily available"

"Joseph King and Natalia Papitashvili for creating the combined OMNI data set"

The OMNI data were downloaded from NASA's Space Physics Data Facility ...

"We thank the reviewers for the careful review of this paper"

The Authors extend their thanks to the referee for important comments and suggestions.

This work was supported by the DLR CGAUSS project

We would like to thank XX for reading drafts of this manuscript...

This work has been done in the frame of the CGAUSS project (url), funded by the DLR

We would like to thank the Helios team and NASA's SPDF for supplying the plasma and magnetic field data (url)

Curriculum vitae

Malte Venzmer, born 5 February 1984 in Bremerhaven, Lower Saxony, Germany, finished secondary school (Abitur) at the Gymnasium Ganderkesee in 2003. Subsequently he performed his civilian service working in a care home for disabled persons in Westerland, Sylt.

In 2004 he began to study physics at the University of Konstanz. During his studies, in summer 2008, he did an internship at the Ångström Laboratory, Uppsala University, Sweden, working in the field of materials physics. In 2010/2011 he wrote his diploma thesis in the *Radio- and X-ray astronomy* group of Dr. Jürgen Kerp at the Argelander-Institute for Astronomy, University of Bonn. There, following his diploma in physics, he continued working under a scholarship until end of 2011.

In 2012 he started as a PhD candidate in the *Solar, heliospheric and space weather research* group of Dr. Volker Bothmer at the Institute for Astrophysics, University of Göttingen. During his doctoral studies he worked as a research assistant for several national and international projects. Most of his main results are described in this very thesis.

notes

Fragen:

- references vol # fett drucken?
- references journal kursiv drucken?
- maybe style references different. like in space science reviews?
- page # oben lassen?
- A5 format?

nice phrases:

...this leads to the question wh... . The answer to this question is developed in the course of the next section.

write basics without third persons view “we”

define if using astronomical symbols...

...and use style consistently

Letzte Änderungen:

Genehmigungen für die Abb. besorgen!!

check for topic sentences!

Am Anfang der Arbeit den folgenden logischen Aufbau der Kapitel erläutern.

Am Anfang jedes Kapitels den folgenden logischen Aufbau der Abschnitte erläutern.

Beides auf Änderungen überprüfen.

print figures to check look of colors

adjust figure width to textwidth...

complete pdfinfo text...

Abkürzungen CME, usw. konsequent nutzen und beim ersten Auftauchen ausschreiben.

englische Kommasetzung beachten!

schauen, ob Komma oder Punkte durch Semikolon ersetzt werden können

Prüfen, ob Überschriften den Inhalt des Kapitels gut beschreiben/gut zum Kapitel passen.

check if AE spelling consistently, search and replace: analyse, etc.

check for thin spaces in numbers with 5 digits and more

Header und footer für notes, seitenzahl, Thema und Kapitel einfügen
check gnuplot plot text sizes and finish figures

check for changed links and update access date

sinnlosen Satz irgendwo einfügen

76 %, ACME irgendwo einfügen (ACME is good...)

comic strip aus thesis extrahieren

put movie in header or footer

create hyperref version including bibtex links

adjust link colors and remove boxes... (hyperref package options)

remove google-books links!

maybe adjust References like in Hathaway2010

LaTeX commands:

block commenting: strg+d

strg+shift+d

$$\frac{T_D}{[K]} = 21,8 \cdot \left(\frac{\Delta v_{FWHM}^{LMC}}{[\text{km s}^{-1}]} \right)^2 \quad (\text{C.7})$$

$$\frac{T_D}{[K]} = 21,8 \cdot \left(\frac{\Delta v_{FWHM}^{LMC}}{[\text{km s}^{-1}]} \right)^2 \quad (\text{C.8})$$

$$k = 3.56 \text{ e-6} \quad (\text{C.9})$$

$$k = 3.56 \cdot 10^{-6} \quad (\text{C.10})$$

$$k = 3.56 \times 10^{-6} \quad (\text{C.11})$$

1. CM LMC Longitude

drei CM LMC Latitude

Volume in $(^{\circ})^2 \text{m s}^{-1}$. Summe aller Voxel des Objektes.

Volume in $(^{\circ})^2 \text{m s}^{-1}$. Summe aller Voxel des Objektes.

- Volume

sdgffs CM GSR Velocity

label

asdf Volume

drei CM LMC Latitude

¹ oder ²

$$a^2 + b^2 = c^2 \quad (\text{C.12})$$

Formel zitieren: (Siehe Formel C.12, Formel (C.12), Seite 84)

package siunitx:
 $20.5 \times 10^{-3} \text{ kg}$
 $20.5 \times 10^{-3} \text{ kg}$
 $20.5 \times 10^{-3} \text{ kg}$

width defines the width of the resulting box as seen from the outside (This means it can be smaller than the material inside the box. You ~~can~~^{can} even set the width to 0pt so that the text inside the box will be typeset without influencing the surrounding boxes). Besides the length expressions, you can also use semi-log plots:

log-lin: logarithmic scale on the y-axis, and a linear scale on the x-axis
lin-log: logarithmic scale on the x-axis, and a linear scale on the y-axis
the naming is output-input (y-x), the opposite order from (x, y)

¹All listed websites were existent on 2008-09-15.

²All listed websites were existent on 2008-09-15.